Development of carbon nanofiber sheet for thermal interface materials and its thermal and mechanical properties

(カーボンナノファイバーを用い熱界面材料用シートの開発とその熱的特性と機械的特性の評価)

XIONG JIANGLING

March 2023

Development of carbon nanofiber sheet for thermal interface material and its thermal and mechanical properties

(カーボンナノファイバーを用い熱界面材料用シートの開発とその熱的特性と機械的特性の評価)

Dissertation for the Degree of

Doctor of Philosophy

Mechanical Engineering Program

Graduate School of Advanced Science and Engineering

Hiroshima University, Japan

Assoc. Prof. Choi Yong Bum, Advisor

XIONG JIANGLING

March 2023

CONTENTS

List of Figures

List of Tables

Chapter 1

Background and objectives

1.1 Introduction

Since the third industrial revolution, the electronics industry has emerged and quickly developed. Especially in the years 1958 to 1975, the introduction of integrated circuits(ICs) with superior capabilities of over several thousand components on a single chip[1]. In the following years, being small in size and light in weight, the ICs has been widely used in electronic components and devices. According to the Moore' law, which is used to predict the number of transistors in a dense ICs double about every two years[2], which means the electronics device continue to show exponential growth in complexity and performance. With rapid development of electronics industry, the size of electronic devices has decreased significantly, but on the contrary the power density goes on increasing. High power, High frequency, high speed of electronic devices greatly increases the overheating problem, the heat dissipation has become a major concern which limited the development of electronics industry. For example, the latest high-end CPU - Intel a Core i9-12900K can consume 125~241W power in a small size of 45mm × 37.5mm. its temperature can hit 373K easily with core-heavy workload, which puts the CPU at risk of shortening and destroying the life of internal components. Thus, the efficient heat dissipation of electronics device is very important, it determines the life and working performance of device itself. In most instances, the electronics device dissipates its heat by contacting metal heat sinks. However, when two solid surfaces are clamped against each other under moderate loading, micro and macroscopic surface defects resulting in the actual contact area being a very small fraction of the apparent contact area[3], which is also called the air gaps. The presence of air gaps results in high thermal resistance and severely reduce the heat dissipation efficiency of the whole electronics device. The thermal interface materials (TIMs) are used to fill the air gaps between heat source and heat sinks, reducing the thermal contact resistance and increasing heat conduction across the interface, which are considered important for improving the heat dissipation efficiency of electronics devices. Mechanically, TIMs must be flexible so that they can conform to mates with uneven surfaces. Meanwhile, the thickness of TIMs must be enough to comply with surface

irregularities and non-planarity. Thermally, TIMs should exhibit high thermal conductivity and low thermal contact resistance[4]. There are many kinds of traditional and commercially available TIMs, the most used ones are thermal grease, phase-change material, thermal pad and metal solder. However, the field of TIM is changing rapidly, these traditional TIMs have many shortcomings and cannot adapt to the requirements of advanced electronic products. Moreover, with the increasing range of human activities, from the land to the depths of the ocean or space, and from hot and dry deserts to cold and humid forests, the use area of the TIMs is also becoming larger and larger. The requirements for TIMs are not only the heat dissipation, but also other functional properties. For example, for electronic equipment used in scientific research in Antarctica, its TIMs need to endure the minimum temperature to 183K[5] and still maintain a good flexibility and thermal conduction ability. For the electronic equipment used in Amazon rainforest with a humid environment of a relative humidity high at an average of 88% in the rainy season and 77% in the dry season[6], TIMs used in this region require a higher humidity resistance than usual. Thus, the development of new TIMs become extremely significant for the heat management of advanced electronic products over the world.

1.2 Types of traditional thermal interface materials (TIMs)

Currently, Thermal grease, phase-change material (PCM), thermal pad and metal solder are the most used traditional TIMs in the world.

Thermal greases, also called thermal pastes or thermal compounds, are the first generation of TIMs and the most widely used in electronics device[7]. Greases have good wetting property, low cost, low assembly pressure. In general, there are types of thermal grease: non-conductive and conductive. Non-conductive thermal grease usually consists of a polymerizable liquid matrix and a large volume fraction of electrically insulating but thermally conductive fillers. Silicone or hydrocarbon oils are often used as matrix material due to their good combination of fluidity and viscosity, allowing more precise filling of air gaps. SiC, Al_2O_3, ZnO and other inorganic material are widely used as thermal conductive filler[8]. The filler loading can be added to 70-80mass% and raise the low thermal conductivity (~0.5 $W \cdot m^{-1} \cdot K^{-1}$)[9] of matrix up to about 5 $W \cdot m^{-1} \cdot K^{-1}$[10] for commercial thermal grease**.** Non-conductive thermal greases have a low price with limited thermal conductivity. Conductive thermal grease types include silver-based, copper-based and aluminium-based thermal grease. These metal-based thermal greases can achieve a higher thermal conductivity than non-conductive thermal grease, Uppal et al. introduced a silicone-oil-based thermal grease through using liquid metal as the filler and micro silver needles to connect the liquid metal droplets[11]. The thermal conductivity of this multiphase thermal grease can reach to 17 $W \cdot m^{-1} \cdot K^{-1}$. But the metal-based thermal greases must be used carefully due to their electronically conductive. They can cause electrical shorts and destroy the electronics if some of them leaks into the ICs. Moreover, all of thermal grease do exhibit various failure mechanisms that can severely impair the functionality of the electronic devices after a long period of use. When two surfaces are subjected to the thermomechanical stress, thermal grease is easily pumped out through the gaps due to its high fluidity and pollute the electronic components. Moreover, at high temperature, the fillers and matrix in thermal grease will be separated, which results in a reduction of thermal

conductivity[12].

PCMs has been widely studied due to their excellent ability to store and release thermal energy[13-15]. PCMs are usually in form of solid state at room temperature and become liquid when the temperature reaches the melting temperature, which can effectively fill the air gap and improve the compliance of TIMs. Moreover, the pump-out problem can also be solved due to the operating temperature of electronics is usually lower than the melting temperature of PCMs in practical applications[16,17]. However, PCMs required a moderate contact pressure to bind surfaces together and their physical and chemical properties are unstable in processes during their long-term usage[18]. Moreover, the high costs, non-electrical insulation and limited heat conduction in solid state are also the disadvantages of PCMs in practical applications.

Typical thermal pads are a kind of thermally conductive silicone elastomer. They are fabricated by directly mixing silicone rubber with thermal conductive fillers or reinforcements depending on the performance requirements, such as ceramic or boron nitride. Due to metal particles are rarely used as fillers, thermal pads are particularly suitable for applications which require an electrical insulation between contact surfaces of electronic devices and heat sinks. Meanwhile, thermal pad could provide better workability and easier assembly process compared to thermal grease, without the concern for pump-out and flexible maintenance during long-term usage. In addition, thermal pad can also act as a vibration damper and protect the electronic devices in mobile state. However, thermal pads usually have a thickness in a range of 200-1000 μm[16,19], which is much higher than other types of TIM. Thus, thermal pads also require high contact pressure(~700kPa)[20] to conform to mating surfaces. Previous research showed that thermal pads should be compressed to at least 25% of their total thickness to deal with the existence of some large air gaps[19]. Other shortcomings of thermal pads are their low thermal conductivity and high thermal contact resistance. A thermal pad with a thermal conductivity of 3 $W \cdot m^{-1} \cdot K^{-1}$ is considered to be the medium quality on the market. Although there are also some commercial thermal pads with a thermal conductivity of 14 $W \cdot m^{-1} \cdot K^{-1}$, they are super high grade and quite expensive[21] that is difficult to apply widely.

Due to compliance in both molten state and solid state, metal solders are widely used

as TIM to enhance the heat conduction between mating surfaces[22-27]. Typical metal solders are low melting-temperature alloys such as bismuth, tin and indium, which have low melting point(333~573K), chemical stability and high thermal conductivity(>30 $W \cdot m^{-1} \cdot K^{-1}$)[28]. In molten state solder can properly fill into the air gap between two mating surfaces, thus, using metal solders with high thermal conductivity can improve the thermal contact conduction efficiently. However, the cost, stress crack and operate complexity involved in metal solders have limited its application for TIM[29].

In addition to the traditional used thermal grease, PCMs, thermal pad and metal solders, there are some other commercially TIMs on the market, such as thermal gels, thermal conductive adhesives and thermal tapes. Fig. 1.1 shows the schematic summary of traditional TIMs and their share market in U.S 2023. Table 1.1 gives the summary of the characteristics, advantages, disadvantages and thermal conductivities of these traditional TIMs.

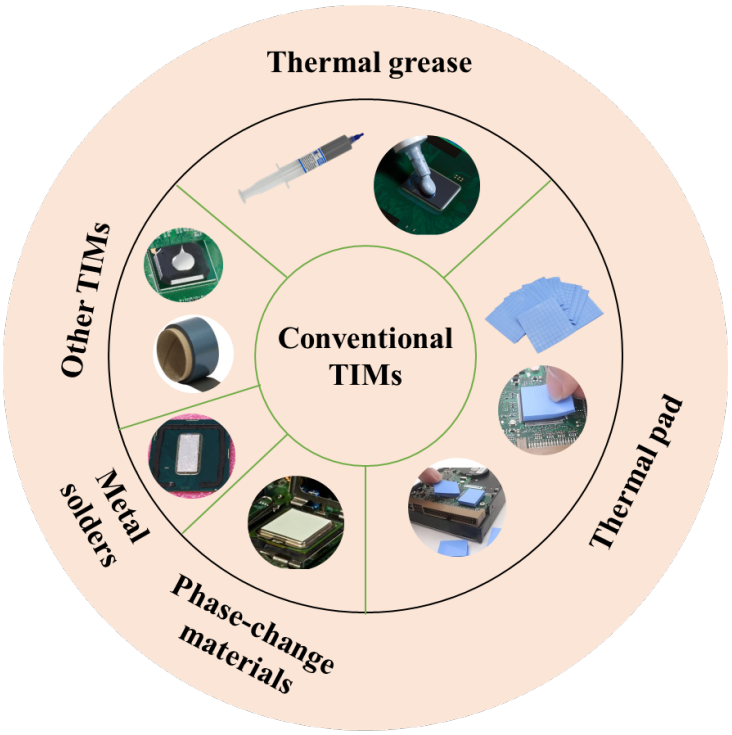

Fig. 1.1 Schematic summary of traditional TIMs and their market share in 2023 U.S.[33]

Table 1.1 The summary of characteristics, advantages and disadvantages of traditional TIMs[16,17,19,29-32].

TIM type	Characteristics	Advantages	Disadvantages	Thermal conductivity [λ/W·m^{-1}·K^{-1}]
Thermal grease	Silicone or hydrocarbon oils + fillers	• Low cost • Good wetting property • Low assembly pressure	• Pump-out effect and dry out • Difficult to control thickness • Hard to maintenance	1-5
Phase-change material	Polyolefin or low molecular weight polymer + fillers	• No pump-out • Easy application than grease • Reusable	• Compressive force required • No electrical insulation	1-5
Thermal pad	silicone rubber + fillers or reinforcements	• No pump-out • Easy application • Electrical insulation	• High thickness • High pressure during installation • More expensive than grease	1-6.5
Metal solder	Low-melt metal alloy	• High thermal conductivity • No pump-out • Mechanical attachment	• High cost • Difficult to install • Corrosion • Void concern	30-86
Thermal gels	Silicone + fillers to form a low module paste	• No pump-out • Reusable • Good wetting property • High temperature stability	• Low thermal conductivity • Cure need • Delamination concern	1-3.5
Thermal conductive adhesives	Silicone or epoxy + fillers	• No pump-out • Low contact resistance • Mechanical attachment	• Cure need • Delamination concern • Low thermal conductivity	1-2
Thermal tapes	Acrylic or silicone-based pressure sensitive adhesive loaded with thermally conductive fillers	• Low cost • No pump-out • Easy to use • Mechanical attachment	• Low thermal conductivity • Hard to fill large air gap efficiently	0.15-0.25

1.3 Development of advanced carbon TIMs

1.3 1 Graphene TIMs

Due to the high thermal conductivity, flexibility and high stability of raw materials, developments on TIM through using carbon materials such as graphene and carbon nanotubes has been widely studied. Graphene, discovered in 2004 by Andre Geim and Konstantin Novoselov, an atomic layer thick carbon with a sp^2 hybrid structure[34]. This material is considered a 21st century materials because of its unique properties and potential for practical application and has attracted researchers from all fields. As showed in Fig. 1.2, graphene has high thermal conductivity (~5300 $W \cdot m^{-1} \cdot K^{-1}$), high mechanical strength (breaking strength of ~42 $N \cdot m^{-1}$ and Young's modules of ~1TPa), high elasticity, flexibility and lightweight properties(Theoretical density of 2.267$g \cdot cm^{-3}$)[34, 36-38]. Although graphene has such excellent properties, it is hard to use it directly due to its 2D structure. Thus, composite with other material such as polymer or metal to fabricate graphene composites is widely studied in recent year. Graphene papers fabricated by stacking graphene nanosheets have been widely reported that have a potential for efficient thermal materials for advanced electronic device[39,40]. Although the graphene bulk composite may achieve a better thermal property, many researchers have turned their attention to the development of graphene paper as TIMs due to its low thickness and flexibility. Graphene paper as a TIM can be used to attach meting surface of heat source and heat sink, achieving a direct contact between the graphene and metal. Based on the ultrahigh in-plane thermal conductivity of graphene paper, feasibility of large-scale preparation and low production cost, the possibility of TIMs for practical application in academia and industry is rising up rapidly[41-43]. In common, according to the types of materials added, graphene TIMs can be simply divided into 4 types: graphene/polymer composite, graphene/metal composite, graphene/other caron material composite, graphene/ceramic composite.

Graphene/polymer composite TIM can achieve a great enhancement of high thermal conductivity at low graphene content, and not significantly affect the intrinsic properties

of the polymer matrix[44,45]. However, due to the bad dispersion of graphene in the polymer and the low thermal conductivity of polymer, although in-plane thermal conductivity is very high to reach 23.5 $W \cdot m^{-1} \cdot K^{-1}$[46], the through-plane thermal conductivity of graphene/polymer composite TIM cannot meet the ideal value(~3 $W \cdot m^{-1} \cdot K^{-1}$)[47].

The use of metal particles with high thermal conductivity to fabricate graphene/metal composite TIM is studied to enhance the through-plane thermal conductivity of TIMs. For example, J. Wang et al. obtained PDA-graphene complexed with metal irons graphene/metal composite, which has a high through-plane thermal conductivity of 3.48 $W \cdot m^{-1} \cdot K^{-1}$[48]. Although metal materials have ultra-high thermal conductivity, the interaction between metal and graphene is relatively weak, resulting in limited through-surface thermal conductivity of composite paper[43].

Enhancing the interaction between the fillers is important to improve the thermal conductivity of graphene TIMs. Compared with other materials, there is no doubt that carbon materials interact better with graphene. An interesting hybrid graphene composite with cellulose nanocrystal added in are reported recently[49]. During the fabricate process, cellulose nanocrystals are carbonized into nanorods after high temperature annealing. These carbon nanorods connect with graphene nanosheet and fill the air gaps in the fabricated composite, which raise the through-plane thermal conductivity to 4.6 $W \cdot m^{-1} \cdot K^{-1}$**.** However, this graphene/nanorods composite material needs an annealing temperature ranging from 1073K to 1773K to achieve the reduction of graphene oxide and carbonization of cellulose nanocrystals[49], which demand a high cost and energy waste during the fabrication process and is hard for practical application. This is also the disadvantages for most graphene/other caron material composite TIMs.

Similar with graphene/metal composite TIM, ceramic materials also can be used as a filler in graphene TIM. Ceramic materials have good thermal conductivity, which is no worse than metal materials. For example, SiC has a thermal conductivity of 80-300 $W \cdot m^{-1} \cdot K^{-1}$ and that of Al_2O_3 is about 30-35 $W \cdot m^{-1} \cdot K^{-1}$[50]. C. P. Feng et al. developed a composite with robust graphene nanoplatelets and large size Al_2O_3 for TIM[51], in which only a single-layer Al_2O_3 particles are distributed in the through-plane direction of this composite and Al_2O_3 particles are covered by graphene nanoplatelets

via simple vacuum-assisted self-assembly method. This graphene/ceramic composite TIM show an excellent through-plane thermal conductivity of 9.09 $W \cdot m^{-1} \cdot K^{-1}$. However, this single-layer structure lack of flexibility and is difficult for large scale production, which is also limited its practical application for TIMs.

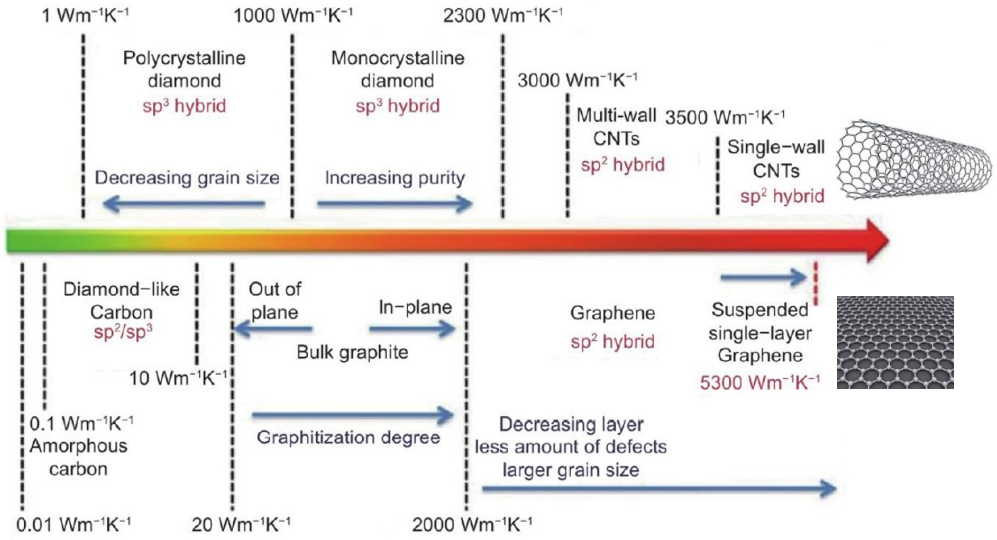

Fig. 1.2 Illustration of thermal conductivities of various carbon materials[35].

1.3 2 Carbon nanotube TIMs

As showed in Fig. 1.2, Carbon nanotube(CNT) can be defined as a rolled-up graphene sheet. Since the discovery of multi-walled CNT(MWCNT) in 1991 by Iijima[52] and single-walled CNT(SWCNT) in 1993 by Iijima and Ichihashi[53], the CNT is considered one of an ideal choice for thermal materials, because of its high thermal conductivity(2800-6000 $W \cdot m^{-1} \cdot K^{-1}$) and mechanical reliability[47,54]. There are many factors There are many factors that affect TC, such as atomic structure, defects, the purity, length and diameter and of the CNTs, especially the length of the CNTs is important for phonon transport and is considered to its increase would contribute to an increase of mean free path for phonons. Heat transfer is carried out by electrons and phonons in solid[55,56]. In common, SWCNT have a longer cylindrical structure and higher purity compared to MWCNT, which contribute to a higher thermal conductivity[57,58].

Many works have been carried out in developing carbon nanotube TIMs. In the First period, researcher just combine CNT and other traditional TIM to seek for a remarkable improvement of thermal conductivity. X. J. Hu et al. introduced a kind of CNT TIM that CNT into a silicone composite filled with metal particles[59]. The thermal conductivity (1.3 $W \cdot m^{-1} \cdot K^{-1}$) of this CNT TIM is about 7 times higher than that of the silicone matrix and 2 times higher than traditional TIMs. Though the thermal conductivity can be improved by adding CNT fillers, many studies have demonstrated that the properties of CNT TIMs cannot be completely exploited[60-63]. The low efficiency is the first reason, due to the random dispersion and discontinuity of CNTs, the heat conduction actually only goes through a small number of CNTs. Thus, heat cannot be conducted directly from a side to the other side through CNTs and the heat conduction would be influenced by matrix with a lower thermal conductivity. Meanwhile, the presence of defects, high thickness, high thermal interface resistance and low purity of CNT is also the reason for low thermal conductivity of CNT TIMs.

Since then, the researchers have explored other way to fabricated CNT TIMs, using

CNT array is considered to be one of the most promising methods. As shown as Fig. 1.3(a), the CNT array, which also call vertically aligned CNTs(VACNTs), is expected provide an efficient thermal conduction because of its highly ordered and vertically aligned structure and a relatively high thermal conductivity of 15~267 $W \cdot m^{-1} \cdot K^{-1}$[63]. M. Wang et al. developed a vertically aligned CNT/epoxy resin composite, which has a high thermal conductivity of 8.23 $W \cdot m^{-1} \cdot K^{-1}$ and good flexibility[64]. As shown as Fig. 1.3(b), H. T. Yu et al. introduced a high thermal conductive and self-healing CNT TIM by using a forest of VACNTs covered by elastic polyimide copolymer[65], which exhibits a high thermal conductivity at 10.83 ± 0.22 $W \cdot m^{-1} \cdot K^{-1}$ and low thermal resistance at 6.83 ± 0.15 $K \cdot mm^2 \cdot W^{-1}$. However, there are still some disadvantages for the usage of CNT array. Firstly, poor thermal/mechanical contact between CNT array and surrounding surfaces resulting in an increasement of thermal contact resistance between CNT array and mating surfaces. In addition, due to the low self-supporting strength of CNT array, they are easily damage during fabricating process(>973K, harsh chemical, long exposure time) or external working environment, such as complex mechanical environment and humid environment[66-68]. Thus, to fully use the excellent thermal properties of CNT array, more research is needed.

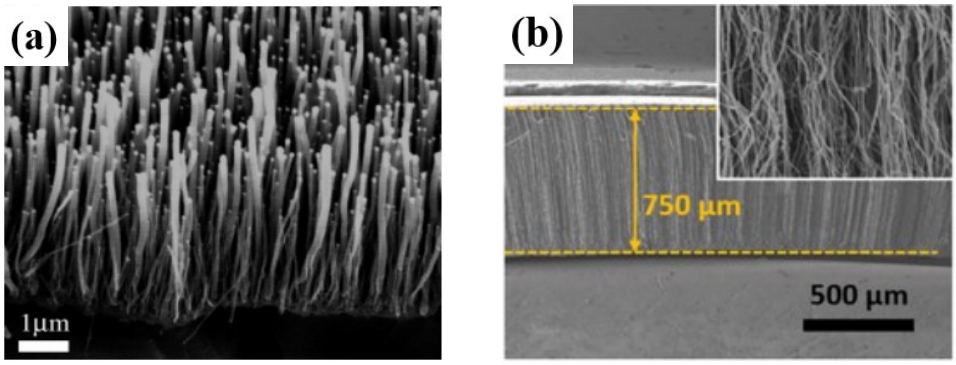

Fig. 1.3 SEM image of (a) vertically aligned CNTs(VACNTs)[69] and (b) an elastic polyimide copolymer and vertically aligned CNT TIM[65].

1.3 3 Carbon fiber TIMs

Among the carbon materials, carbon fiber(CF) is the oldest one which discovered in the mid-1800s by J. W. Swan[70]. Similar to graphene and CNT, CF has many excellent properties like high strength, high thermal and chemical stabilities, low density and good thermal and electrical conductivities. However, , CF is often used to composite with metal materials and seldom to be studied for TIM application due to its structure limitations and low relative thermal conductivity(190-220 $W \cdot m^{-1} \cdot K^{-1}$) compared to graphene and CNT. As shown in Fig. 1.4, the group of J. K. Ma et al. developed a 3D network of CFs composited in epoxy polymer where CFs is randomly dispersed[71]. This CF/epoxy TIM provided an enhanced through-plane thermal conductivity(2.84 $W \cdot m^{-1} \cdot K^{-1}$) compare with epoxy matrix(0.19 $W \cdot m^{-1} \cdot K^{-1}$). However, the thermal conductivity is still lower than commercial TIM and further improvement is needed. And then, similar to VACNT, to solve the low thermal conductivity of CF composite, vertically aligned CFs are also used for developing new TIM. Recently, Q. Wu et al. reported that a kind of CF reinforced elastomeric TIM. In the fabrication process, on the basis of conventional alumina/silicone rubber, mesophase pitch CFs are added as fillers and the CFs are oriented in the matrix by a strong magnetic field during the fabrication process[72]. In their report, the composite with 20 vol% CFs shows an outstanding thermal conductivity of 26.49 $W \cdot m^{-1} \cdot K^{-1}$. However, due to the flexible fabrication process and the necessity to use magnetic field treatments, it is difficult for the practical application. Improving the thermal conductivity is not the only requirement for developing a new TIM, reducing the cost, simplifying the fabrication process and allowing for big scale industrial production are also important issues for researchers to consider. As a type of carbon nanofiber, vapor grown carbon fiber(VGCF, CNF) has excellent mechanical properties such as high thermal conductivity, high specific strength, and high corrosion resistance and is commercially available at a low cost. VGCF can be incorporated in a wide range of matrices, including thermoplastics and thermosets, for the formation of thin and flexible sheets. Thus, VGCF is considered an

ideal material for TIM development in this study.

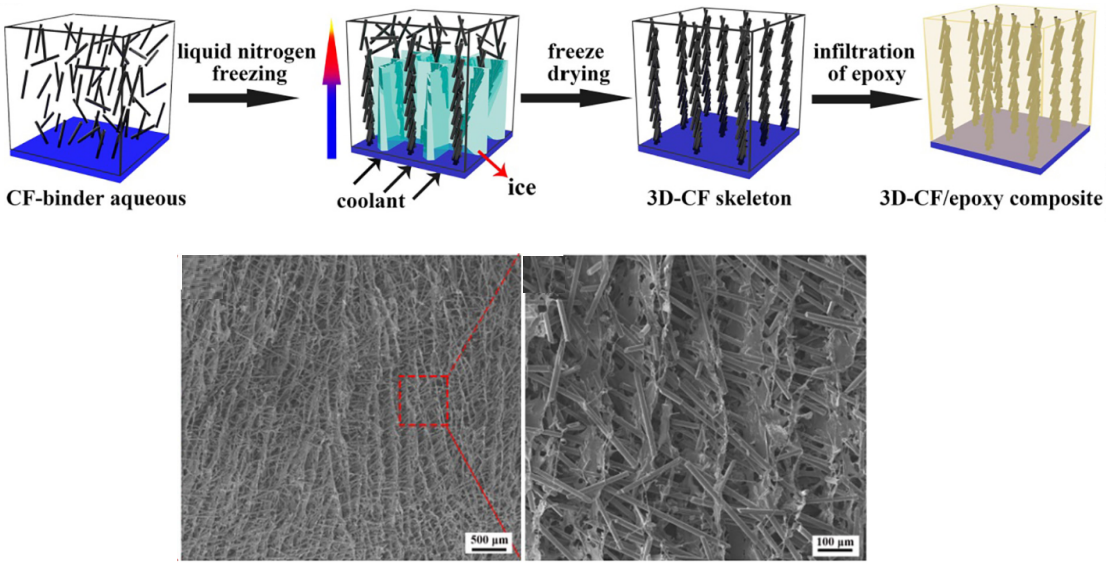

Fig. 1.4 Schematic of fabrication and microstructure of 3D carbon fiber skeleton/epoxy resin composite TIM.

1.4 Fabrication methods of TIMs

There are many fabrication methods for different types of TIMs, and researchers are still exploring some new method now. To traditional TIMs like thermal grease, PCM and thermal pad, direct incorporation method is most widely to be used in industrial production which described as mixing the fillers into matrix directly, then follows the pelletize, compress, dry and heating process if it is necessary[73]. Metal solders is applied on the mating surface by soldering. To carbon TIMs, the fabrication method can be much more diverse and selective thanks to the flexibility and chemical and thermal stability of carbon material, such as vacuum filtration(VF), solution casting, layer-by-layer assembly, chemical vapor deposition(CVD), electro-spray deposition(ESD), freeze casting and so on. Among these fabrication methods, VF and solution casting are the most commonly used and relatively simple ones. In the VF process, the homogeneous dispersion of carbon material, other fillers and solvent is vacuum filtrated by using a filter. After removing the filter and drying under the right conditions, a TIM film will be obtained. And solution casting is an easier and low-cost method to fabricate TIMs, which can also be applied to large scale TIM products in practical applications. Table 1.2 shows a simple summary of fabrication method of advanced carbon TIMs.

Table 1.2 The summary of fabrication method of advanced carbon TIMs.

Sample	Fabrication method	Thermal conductivity [λ/W·m^{-1}·K^{-1}]		Year [Ref]
		In-plane	Through-plane	
BN nanosheet/cellulose nanofiber	Vacuum filtration	22.67	1.08	2018[74]
CNF/RGO	Vacuum filtration	7.3	0.13	2017[75]
CNTs/RGO	Vacuum filtration	977	0.38	2014[76]
AgNPs@BC/Al_2O_3/GNPs	Vacuum filtration	27.78	9.09	2022[51]
RGO paper	Solution casting	61	0.09	2015[77]
PVDF/BN/GNPs	Solution casting	unknown	0.72	2018[78]
Cellulose/GNP	Solution casting	800	5.5	2018[79]
NFC/RGO	Layer by layer assembly	12.6	0.042	2017[80]
Epoxy/VACNTs	CVD	unknown	1.65	2019[81]
SiC/CF	CVD	unknown	16.8	2017[82]
Epoxy/CNT	CVD	1	4.87	2011[83]
Epoxy/Graphene network	Freeze casting	unknown	2.13	2016[44]
Epoxy/Carbon fiber network	Freeze casting	1.7	2.84	2020[71]

BN: Boron nitride RGO: Reduced graphene oxide GNP: Graphene nanoplatelet AgNPs: silver nanoparticles
BC: Bacterial cellulose PVDF: Polyvinylidene fluoride

1.5 Computer-assisted thermal simulations of TIM.

As a new trend of current science research, combining computer simulation and practical experiments together become an important way to study new things and demonstrate new ideas. Compared to experiments, simulations can help researchers to generate new knowledge and thoughts about unknown territory by a simpler and more intuitive way. Recently, computer-assisted thermal simulations of advanced TIM using finite element analysis(FEA) software begin to appear commonly in research. FEA is a computerized method for predicting the how real objects will respond to force, heat, vibration and other physical effects under the specified conditions set by people. The working principle of FEA is to break down real objects into a large number of finite elements and use mathematical equations help predict the behavior of each element. And in final, the results of each element will be summed up to predict the behavior of the whole object[84]. Using thermal simulation by FEA could contribute to a significant reduction of development circles, avoidance of material waste and lower research cost. For example, as shown as Fig. 1.5, W. Dai et al. build an evaluation system of Heater-TIM-Heat sink to investigate and compare the cooling performance between their developed new graphene TIM and state-of-the-art TIMs in real case[85]. However, like most thermal simulation of TIM, the microstructure of their developed TIM and the arrangement of graphene are not considered, the model of TIM is created as an equivalent to a single-phase material with uniform internal structure. As another example, Q. Q. Ma et al. develop an aluminum/polymer TIM and through the usage of FEA to study the uniform temperature distribution along the heat transfer path of this TIM[86], which is showed in Fig. 1.6. In the reported studies, the computer-assisted thermal simulation and analysis of fiber reinforced composite materials is seldom to be studied, due to the complicated and different arrangement of fibers in each research.

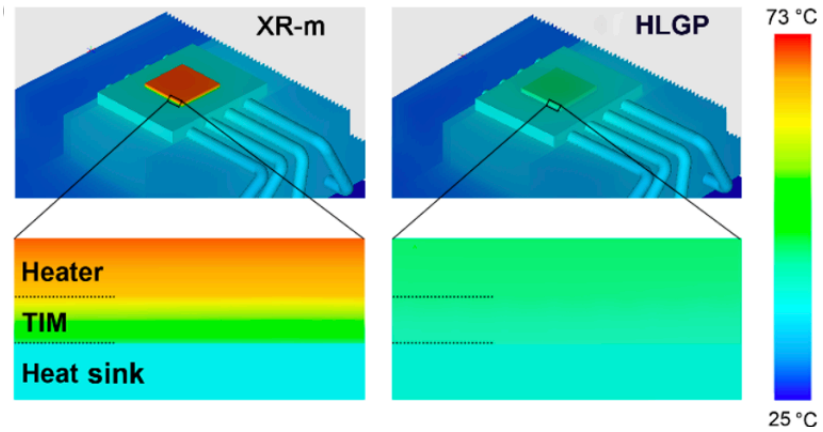

Fig. 1.5 Temperature distribution comparison of commercial TIM(XR-M) and developed new graphene TIM(HLGP)[88].

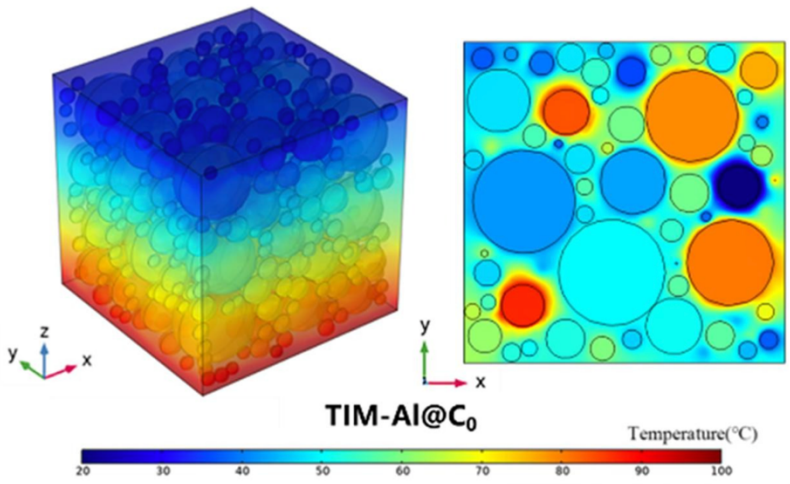

Fig. 1.6 Temperature distribution and cross-sectional view of Aluminum/polymer TIM filled in a typical heating process.[89].

1.6 Problem of previous studies and objectives of this study

As mentioned above, traditional TIMs cannot meet the requirements of electronic devices with a high-speed development, due to their low thermal conductivity and other poor properties, such as the pump-out of thermal grease and the poor stability during long-term usage of PCMs. In the previous studies, although advanced carbon TIMs are developed successfully with higher thermal conductivity, light-weight property, better physical and mechanical stability compared to traditional TIM, the properties of developed carbon TIMs still cannot not be completely exploited and failed to meet the design value temporarily. Besides, the balance between performance and cost of TIM should concerned as another key. Using high-cost material and complicated fabrication process may contribute to a higher thermal conductivity or other important properties of advanced carbon TIM, but it is unfavorable to practical application and industrial production.

In this study, VGCF and polyvinyl alcohol(PVA) were fabricated to CNF sheets that exhibit high thermal conductivity through a simple fabrication method. PVA, a commercial resin, is expected to bind VGCFs and impart high flexibility to fabricated sheets through its high adhesion strength and high malleability. The microstructure was observed, and the thermal and mechanical properties of fabricated sheets were investigated. Moreover, as an attempt to increase the functionality of fabricated CNF sheets for practical application, polytetrafluoroethylene (PTFE) was added to fabricated PVA-PTFE-VGCF sheets for an improvement in hydrophilicity. The effect of PTFE addition on microstructure and properties of CNF sheet were discussed. In addition, the thermal simulation was also carried out with the purpose of investigating the heat transfer path in CNF sheet. Our purpose was to fabricate a CNF sheet that exhibit high thermal conductivity by a simple and low-cost fabrication process for advanced TIM applications.

1.7 Outline of this study

In Chapter 1, types of traditional TIMs were introduced and the development of advanced carbon TIMs was reviewed. The requirements properties of TIM and the problems of the existed TIM were also discussed.

Chapter 2 introduced the fabrication of the PVA-based CNF sheet for TIM by solution casting method. The microstructure, porosity, thickness, density, hardness and thermal conductivity were discussed. In addition, high temperature and humidity test was measured in this chapter.

Chapter 3 introduced the fabrication of PVA-PTFE-VGCF sheet. By using two types of PTFE with different size, the effect of PTFE addition on microstructure, thermal conductivity and other properties of CNF sheet were investigated.

In Chapter 4, the thermal simulation of PVA-VGCF sheet is measured by using FEA ANSYS student software. 5 types of microstructure models were created as: pure PVA, horizontally arranged VGCF in PVA, vertically arranged VGCF in PVA and randomly arranged VGCF in PVA, respectively. The heat transfer path inside the models is briefly evaluated and the thermal conductivity of them was calculated through using the simulation results.

As last, the results from the above-mentioned studies are summarized in Chapter 5.

References

[1] J. S. Kilby: IEEE Trans. Electron Devices **23** (1976) 648-654.

[2] S.E. Thompson, S. Parthasarathy: Mater. Today **9** (2006) 20–2.

[3] A. Bejan, A. D. Kraus: Heat transfer handbook, (John Wiley & Sons, Inc., Hoboken, New Jersey, 2003) pp. 4-7

[4] J. Due, A. J. Roinson: Appl. Therm. Eng. **50** (2013) 455-463.

[5] Encyclopædia Britannica, Inc., USA, Available at. https://www.britannica.com/place/Antarctica/Plant-life (Accessed 2022-11-26).

[6] World Wide Fund For Nature, Switzerland, Available at. https://wwf.panda.org/discover/knowledge_hub/where_we_work/amazon/about_the_amazon/ (Accessed 2022-11-26).

[7] L. S. Fletcher: IEEE Trans. Compon. Hybrids Manuf. Technol. **13** (1990) 1012-1021.

[8] W. K. Xing, Y. Xu, C. Y. Song, T. Deng: Nnanomaterials **12** (2022) 3365.

[9] W. Haller et al.: Ullmann's Encyclopedia of Industrial Chemistry, (Wiley, New York, 2014) pp. 58-59.

[10] RS Components Pty Ltd., UK, Available at. https://au.rs-online.com/web/c/hvac-fans-thermal-management/electronics-heating-cooling-components/thermal-grease/ (Accessed 2022-11-26).

[11] A. Uppal, W. Kong, A. Rana, R.Y. Wang, K. Rykaczewski: ACS Appl. Mater. Interfaces **13** (2021) 43348-43355.

[12] B. Wunderle, D. May, J. Heilmann, J. Arnold, J. Hirscheider, Y. Li, J. Bauer, R. Schacht, M. A. Ras: In Proceedings of the 2019 20th International Conference on Thermal (2019) pp. 24-27.

[13] J. Yang, L. S. Tang, R. Y. Bao, L. Bai, Z. Y. Liu, B. H. Xie, M. B. Yang, W. Yang: Sol. Energy Mater. Sol. Cells **174** (2018) 56-64.

[14] Y. Liu, R. W. Zheng, J. Li: Renew. Sust. Energ. Rev. **168** (2022) 112783.

[15] J. Yang, G. Q. Qi, L. S. Tang, R. Y. Bao, L. Bai, Z. Y. Liu, W. Yang, B. H. Xie, M.

B. Yang: J. Mater. Chem. **4** (2016) 9625-9634.

[16] X. C. Tong: Advanced Materials for Thermal Managment of Eletronic Packaging, (Spring, New York, 2011) pp. 343-346.

[17] C. P. Feng, L. Y. Yang, J. Yang, L. Bai, R. Y. Bao, Z. Y. Liu, M. B. Yang, H. B. Lan, W. Yang: Compos. Commun. **22** (2022) 100528.

[18] Y. Li, G. Sang, H. Shi: J. New mater. Electrochem. Syst. **17** (2014) 123-127.

[19] R. Viswanath: Intel technology journal **3** (2000) 1.

[20] D. Blazej, Available at. http://www.electronics-cooling.com/2003/11/thermal-interface-materials/ (Accessed 2022-11-26).

[21] A. Gobor, Available at. https://www.ekwb.com/blog/thermal-compound-guide/#:~:text=A%20thermal%20pad%20with%203W,high%20grade%20and%20quite%20expensive. (Accessed 2022-11-26).

[22] D. D. L. Chung: Mater. Eng. Perform. **10** (2001) 56-59.

[23] S. J. Subramanian: International Eletronic Packaging, parts A, B, and C, ASME. (2005) pp. 959-963.

[24] S. A. Fleischer, L. H. Chang, C. B. Johnson: Microelectron Reliab. **46** (2006) 794-804.

[25] L. Ciampolini, M. Ciappa, P. Malberti, P. Regli, W. Fichtner: Microeletronic J. **30** (1999) 1115-1123.

[26] F. Hua, C. Deppisch, T. Fitzgerald: IMAPS. Advancing microeletronics (2006) pp. 16-17.

[27] X. Hu, L. Jiang, K. E. Goodson: Semiconductor thermal measurement and managment symp, IEEE (2004) pp. 98-103.

[28] W. X. Chu, P. H. Tseng, C. C. Wang: Appl. Therm. Eng. **163** (2019) 114438.

[29] R. Prasher: Historical perspective, status, and future directions, IEEE (2006) pp. 1571-1586.

[30] J. Yang, L. S. Tang, R. Y. Bao, L. Bai, Z. Y. Liu, W. Yang, B. H. Xie, M. B. Yang: Chem. Eng. Sci. **315** (2017) 481-490.

[31] F. Sarvar, C. D. Whalley, P. P. Conway: Electronics system integration technology conference, IEEE (2006) pp. 1292-1302.

[32] J. P. Gwinn, R. L. Webb: Microeletron J. **34** (2003) 215-222.

[33] Grand View Research Inc., USA, Available at. https://www.grandviewresearch.com/industry-analysis/thermal-interface-materials-market (Accessed 2022-11-26).

[34] K. S. Novoselov, A. K. Geim, S. V. Morozov, D. Jiang, Y. Zhang, S. V. Dubonos, I. V. Grigorieva, A. A. Firsov: Science **306** (2004) 666-669.

[35] H. L. Li, S. N. Xiao, H. L. Yu, Y. H. Xue, J. H. Yang: New Carbon Mater. **36** (2021) 897-910.

[36] C. Lee, X. D. Wei, J. W. Kysar, at al.: Science **321** (2008) 385-388.

[37] A. K. Geim, K. S. Novoselov: Nat. Mater. **6** (2007) 183-191.

[38] K. S. Novoselov, A. K. Geim, S. V. Morozov, D. Jiang, Y. Zhang, M. I. Katsnelson, I. V. Grigorieva, S. V. Dubonos, A. A. Firsov: Nature 438 (2005) 197-200.

[39] L. Peng, Z. Xu, Z. Liu: Advanced Material **29** (2017) 1700589.

[40] H.Y Sun et al.: Chem. Mater. **29** (2017) 7808-7815.

[41] C. Kim, S. An, J. Lee: ACS Appl. Mater. Interfaces **11** (2019) 924-929.

[42] H. Malekpour, K. H. Chang, J. C. Chen, C. Y. Lu, D. L. Nika, K. S. Novoselov, and A. A. Balandin: Nano letters **14** (2014) 5155-5161.

[43] L. Lv, W. Dai, J. H. Yu, N. Jiang, C. T. Lin: New Carbon Mater. **36** (2021) 930-939.

[44] G. Lian, C. C. Tuan, L. Li, S. Jiao, Q. Wang, K. S. Moon, D. Cui, C. P. Wong: Chem. Mater., **28** (2016) 6096-6104.

[45] X. H. Li, P. Liu, X. Li, F. An, P. Min, K. N. Liao, Z. Z. Yu: Carbon, **140** (2018) 624-633.

[46] H. Fang, Y. Zhao, Y. Zhang, Y. Ren, S.L. Bai: ACS Appl. Mater. Interfaces **9** (2017) 26447-26459.

[47] J. Khan, S. A. Momin, M. Mariatti: Carbon **168** (2022) 65-112.

[48] J. Wang, P. G. Ren, Z. Y. Chen, T. Wu, F. F. Wang, C. Y. You: Appl. Surf. Sci. **610** (2023) 155309.

[49] X. Meng, H. Pan, C. L. Zhu, Z. X. Chen, T. Lu, D. Xu, Y. Li, S. M. Zhu: ACS Appl. Mater. Interfaces **10** (2018) 22611-22622.

[50] LINSEIS, USA, Available at. https://www.linseis.com/en/applications/ceramics-and-glass-industry/lfa-1000-aluminum-oxide-al2o3-thermal-diffusivity-

conductivity/ (Accssed 2022-11-26).

[51] C. P. Feng et al.: Chem. Eng. J. **392** (2020) 123784.

[52] S. Iijima: Nature **354** (1991) 56-58.

[53] S. Iijima, T. Ichihashi: Nature **363** (1993) 603-605.

[54] Y. Gogotsi: Nanotubes and Nanofibers (CRC Press, New York, 2006) pp. 51-58.

[55] S. Maruyama: Microscale Thermophs. Eng. **7** (2003) 41-50.

[56] M. Maldovan: Nature **503** (2013) 209-217.

[57] E. Pop, D. Mann, Q. Wang, K. Goodson, H. Dai: Nano Lett. **6** (2006) 96-100.

[58] Z. Han, A. Fina: Prog. Polym. Sci. **36** (2011) 914-944.

[59] X. J. Hu, L. N. Jiang, K.E. Goodson: ITHERM'04, IEEE (2004) pp. 63-69

[60] X. J. Hu, A. Antonio, J. Xu, T. S. Fisher, K. E Goodson: J. Heat Transf. **128** (2006) 1109-1113.

[61] N. Greef et al.: Diamond Relat. Mater. **51** (2015) 39-48.

[62] K. Zhang, M. M. Yuen, N. Wang, J. Y. Miao, D. G. Xiao, H. B. Fan: Electronic components and technology conference, IEEE (2006) pp. 177-182.

[63] W. Yu, C. Liu, S. Fan: Nano Research **14** (2021) 2471-2490.

[64] M. Wang, H. Y. Chen, W. Lin, Z. Li, Q. Li, M. H. Chen, F. C. Meng, Y. J. Xing, Y. G. Yao, C. P. Wong, Q. W. Li: Appl. Mater. Interfaces **6** (2014) 539-544.

[65] H. T. Yu, Y. Y. Feng, C. Chen, Z. X. Zhang, Y. Cai, M. M. Qin, W. Feng: Carbon **179** (2021) 348-357.

[66] Z. J. Dong, B. Sun, H. Zhu, G. M. Yuan, B. L. Li, J. G. Guo, X. K. Li, Y. Cong, J. Zhang: New Cabon mater. **36** (2021) 873-895.

[67] M.T. Barako, Y. Gao, Y. Won, A.M. Marconnet, M. Asheghi, K.E. Goodson: IEEE Trans. Compon. Packag. Manuf. Technol. **4** (2014) 1906-1913.

[68] Y. Gao, A.M. Marconnet, M.A. Panzer, S. Leblanc, S. Dogbe, Y. Ezzahri, A. Shakouri, K.E. Goodson: J. Electron. Mater. **39** (2010) 1456-1462.

[69] Q. Ngo, B. A. Cruden, A. M. Cassel, G. Sims, M. Meyyappan, J. Li, C. Y. Yang: Nano letters **4** (2004).

[70] VHR Inc., UK, Available at. https://blog.v-hr.com/blog/history-of-engineering-carbon-fibre. (Accssed 2022-11-26).

[71] J. K. Ma, T. Y. Shang, L. L. Ren, Y. M. Yao, T. Zhang, J. Q. Xie, B. T. Zhang, X.

L. Zeng, R. Sun, J. B. Xu, C. P. Wong: Chem. Eng. J. **380** (2020) 122550.

[72] Q. Wu, W. J. Li, C. Liu, Y. W. Xu, G. G. Li, H. X. Zhang, J. Y. Huang, J. Y. Miao: Carbon **187** (2022) 432-438.

[73] Z. Jiang, M. E. N. Rivero, A. Anagnostopoulos, X. H. She, X. L. Liu, Y. M. Xuan, Y. L. Ding: Power Technology **391** (2021) 533-556.

[74] Z. R. Hu, S. Wang, G. K. Chen, Q. Zhang, K. Wu, J. Shi, L. Y. Liang, M. M. Lu: Compos. Sci. Technol. **168** (2018) 287-295.

[75] W. X. Yang, Z. D. Zhao, K. Wu, R. Huang, T. Y. Liu, H. Jiang, F. Chen, Q. Fu: J. Mater. Chem. C. **5** (2017) 3748-3756.

[76] Q. Q. Kong et al.: Adv. Funct. Mater. **24** (2014) 4222-4228.

[77] J. D. Renteria, S. Ramirez, H. Malekpour, B. Alonso, A. Centeno, A. Zurutuza, A. I. Cocemasov, D. L. Nika, A. A. Balandin: Adv. Funct. Mater. **25** (2015) 4664-4672.

[78] Q. Song, W. Zhu, Y. Deng, D. He, J. Feng: Compos. Sci. Technol. **168** (2018) 381-387.

[79] M. Zahid, M.T. Masood, A. Athanassiou, I.S. Bayer: Appl. Phys. Lett. **113** (2018) 044103.

[80] N. Song, D. J. Jiao, S. Q. Cui, X. S. Hou, P. Ding, L. Y. Shi: ACS Appl. Mater. Interfaces **9** (2017) 2924-2932.

[81] B. Shan, G. Yuan, H. Li, J. Liu: Jpn. J. Appl. Phys. **58** (2019) SHHH01.

[82] S. C. Chen, Y. Y. Feng, M. M. Qin, T. X. Ji, W. Feng: Cabon **116** (2017) 84-93.

[83] A. M. Marconnet, N. Yamamoto, M. A. Panzer, B. L. Wardle, K. E. Goodson: ACS Nano **5** (2011) 4818-4825.

[84] Autodest Inc., USA, Available at. https://www.autodesk.com/solutions/finite-element-analysis (Accssed 2022-11-26).

[85] W. Dai et al.: ACS Nano **13** (2019) 11561-11571.

[86] Q. Q. Ma et al.: Compos. Part A **157** (2022) 106904.

Chapter 2

Development of polyvinyl alcohol-based carbon nano fiber sheet

2.1 Introduction

With the continually development of electronic industry, the heat density is increasing rapidly on the electronic components. Without efficient heat dissipation, malfunctions would be happened in junctions or modules of electronic component caused by heat concentration[1]. Therefore, efficient heat dissipation threatens to limit not only the working performance but also the service life of electronic component. Thermal interface materials (TIMs), which is used to fill the air gaps between electronic component and heat sink, are generally considered as an important part to improve the heat dissipating efficiency of electronic device by increasing the thermal conductive and reducing the thermal contact resistance on the contact surface between electronic component and heat sink. There are many types of TIM materials such as thermal pad, phase change materials, graphite sheets and metal sheets[2]. Grease is generally used as TIM at present, but there were problems such as the difficulty of uniform spread and the inclusion of voids in the grease. If grease is not properly spread, heat conduction from the heat source to the heat sink could not be efficiently performed. The phase change materials require a moderate contact pressure to keep mating surfaces together, in addition, the physical and chemical properties of the phase change materials are not stable during long term use[3]. In recent years, new TIM development has been promoted by carbon material, like Graphene, Carbon nanotube (CNT), Carbon nanofiber (CNF) and others. Carbon materials such as graphene and CNTs, have been widely studied as the fillers of TIMs, because of their high thermal conductivity and excellent mechanical properties[4-8]. However, due to 2-dimensional structure, graphene TIMs have a strongly anisotropic thermal conductivity. For example, Jeon et al. developed a new cellulose-graphene-based TIM papers[9]. According to their report, although the in-plane thermal conductivity of the cellulose-graphene-based TIM paper was 7.32 $W \cdot m^{-1} \cdot K^{-1}$, the maximum through-plane thermal conductivity was very low which was only 0.14 $W \cdot m^{-1} \cdot K^{-1}$. Huang et al. reported thermal conductivities of current advanced graphene-based polymer composites. The thermal conductivities of most

reported graphene-based polymer nanocomposites were under 10 $W \cdot m^{-1} \cdot K^{-1}$, using graphene to enhance thermal conductivity did not show significant effect due to the high aspect ratio of graphene materials[7]. As for CNT TIMs, many studies have demonstrated that it is hard to reach the expected properties, because of defects, thickness, interface thermal resistance and purity[10]. Hong et al. fabricated a new CNTs/polymethylmethacrylate (PMMA) composite by using single-walled carbon nanotubes (SWCNTs) and multi-walled carbon nanotubes (MWCNTs). The maximum thermal conductivity of SWCNT/PMMA and MWCNT/PMMA composites were only 2.43 $W \cdot m^{-1} \cdot K^{-1}$ and 3.44 $W \cdot m^{-1} \cdot K^{-1}$. Their reports stated that the thermal conductivity of CNT TIMs was significantly affected by the purity and defects of CNT[11]. Moreover, the commercialization of most advanced TIMs is difficult due to the complexity in large-scale manufacturing method and their high cost. As for another carbon material, CNF are discontinuous, highly graphitic, highly compatible with most polymer processing techniques, and they can be dispersed in an isotropic or anisotropic mode. As a type of CNF, vapor grown carbon fiber (VGCF) has excellent mechanical properties, such as high thermal conductivity, high specific strength, corrosion resistance, and it is a commercially available carbon material with low price. VGCF can be imparted to a wide range of matrices including thermoplastics and thermoset to form thin and flexible sheets. Therefore, carbon nanofiber was chosen as thermally conductive fillers instead of other carbon materials. As a resin, PVA is expected to bind VGCFs together and provide a good flexibility to CNF sheet, due to a good adhesiveness and film-forming property.

The objective of this chapter is to fabricate PVA-based CNF sheets that exhibit high thermal conductivity and good workability by a simple and low-cost fabrication process. The microstructure of the PVA-VGCF sheets was determined through scanning electron microscopy (SEM), and their porosity was calculated by using an image analysis software. The thickness, density, and hardness of the PVA-VGCF sheets were also investigated. A periodic heating and infrared radiation thermometer method was used to measure the thermal conductivities of the PVA-VGCF sheet. In addition, a high temperature and humidity tests was measured to investigate the long-term performance of PVA-VGCF sheet, the test condition was set as 358 K and 85% RH for 500 h.

2.2 Experimental procedure

2.2.1 Raw materials

In this study, VGCFs with a diameter of 150nm and length of 10-20μm (Showa Denko Co., Ltd.) were used for enhancing the thermal conductivity of fabricated sheet, and a commercial PVA solution(Yamato Co., Ltd) with a concentration of 13 mass% sold was used as the binder. SEM image of as-received VGCF and general chemical formula of PVA are shown in Fig. 2.1. It should be noted that although the VGCFs was readily aggregates, the VGCFs were used under as-received condition directly, no dispersion medium was used in this study. Because the aggregation of VGCFs can contribute to provide a 3D net-like structure during the fabrication process, which is expected to improve the isotropic thermal conductivity of fabricated sheets.

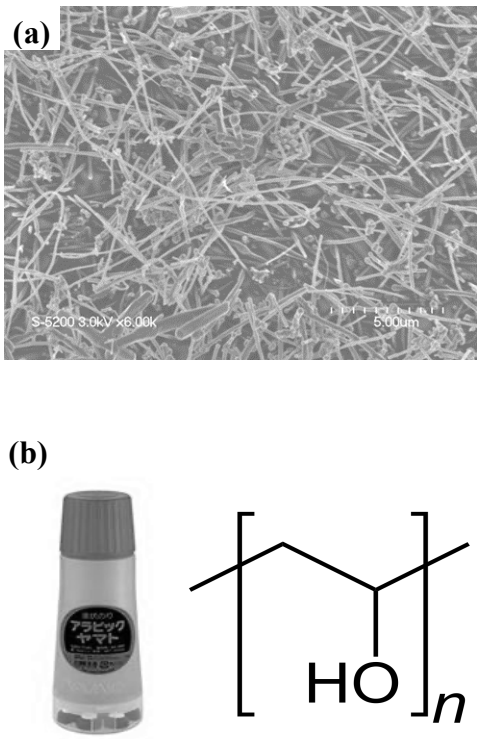

Fig. 2.1 (a) FE-SEM image of VGCFs, and (b) Image and chemical formula of PVA.

2.2.2 Fabrication method of PVA-VGCF sheet

The fabrication procedure of CNF sheet is shown in Fig. 2.2. First, in order to obtain a TIM sheet with an isotropic thermal conductivity, the as-received VGCFs was poured into PVA binder directly without any dispersion medium. After mixing by a silicone bar with 20 rpm for 1 minute, spread the VGCF-PVA mixture on a PET ($(C_{10}H_8O_4)n$) film which is A4 paper size. Then, dried at room temperature (RT) for 48hours, the CNF sheet can be separated from PET film. In this study, to investigate the influence of amount of VGCF on thermal conductivity, five types of CNF sheets were fabricated with different the weight ratio of VGCF under fixed PVA amount. The fabrication conditions of CNF sheets are shown in Table 2.1.

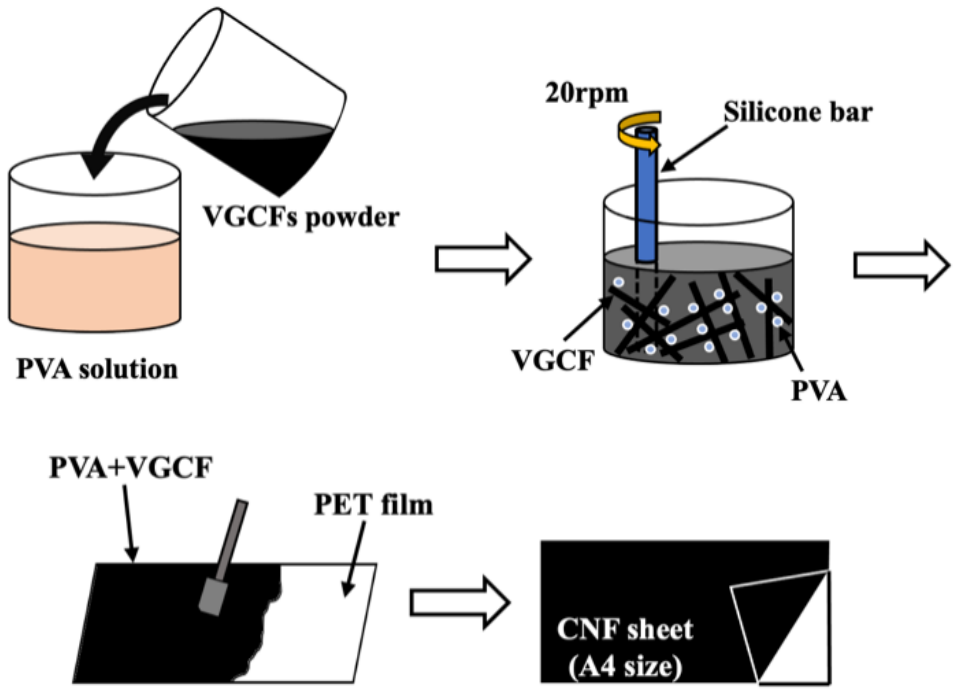

Fig. 2.2 Schematic of the fabrication procedure of CNF sheet.

Table 2.1 Fabrication conditions of PVA-VGCF sheets.

Samples	PVA: VGCF (mass%)	VGCF (mass%)	VGCF (vol.%)
a	1:0.100	43.48	17.04
b	1:0.070	33.90	12.85
c	1:0.050	27.78	10.15
d	1:0.030	20.41	8.18
e	1:0.025	16.13	7.95

2.2.3 Evaluation methods and equipment

2.2.3.1 Observation of microstructure

The microstructure of PVA-VGCF sheets were characterized by field mission scanning electron microscopy (FE-SEM, HITACHI, S-5200).

2.2.3.2 Measurement of porosity, thickness, density and hardness

The porosity of each sheet was calculated by image analysis using the Image Pro Plus 6.0, and 5 random areas with a size of 250μm^2 in each PVA-VGCF sheet was used for image analysis. The density was calculated by mass and volume of each fabricated sheet. The hardness of PVA-VGCF sheets was also tested by a shore durometer. According to ASTM D2240 procedure, the PVA-VGCF sheets with a total thickness of 5 mm were used for hardness measurement.

2.2.3.3 Periodic heating and infrared radiation thermometer method for thermal conductivity

The thermal diffusivities of the PVA-VGCF sheets were evaluated by using periodic heating and infrared radiation thermometer method at room temperature, with a thermophysical analyzer (Thermowave Analyzer TA, BETHL). Fig. 2.3 shows the schematic of measurement theory. As showed in Fig. 2.4, 5 random points were chosen to measure the thermal diffusivity of a simple with a size of 2500mm^2. The specific heat capacities of CNF sheets were measured by differential scanning calorimetry(DSC, X-DSC7000, HITACHI). After getting all these values, TC was calculated with the equation:

$$\lambda = \alpha \times \rho \times C_p \tag{2.1}$$

where λ is thermal conductivity (W·m^{-1}·K^{-1}), α is thermal diffusivity(×10^{-6}m^2·s^{-1}), ρ is density(×10^{6}g·m^{-3}) and C_p is specific heat capacity(J·g^{-1}·K^{-1}) of samples, respectively.

(a) In-plane direction

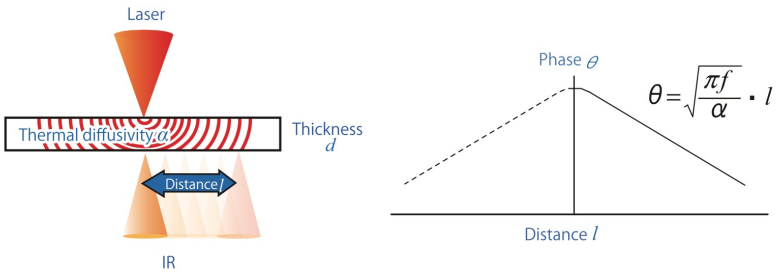

(b) Through-plane direction

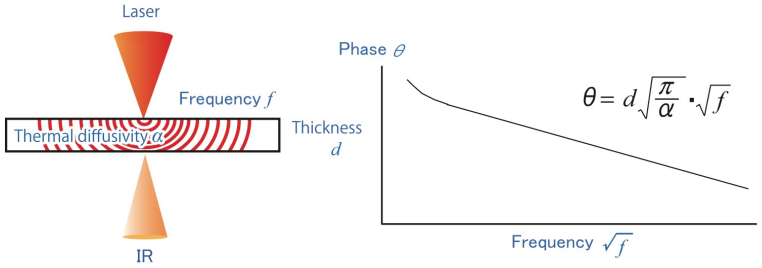

Fig. 2.3 Schematic of theory of periodic heating and infrared radiation thermometer method: (a) In-plane direction (b) Through-plane direction.

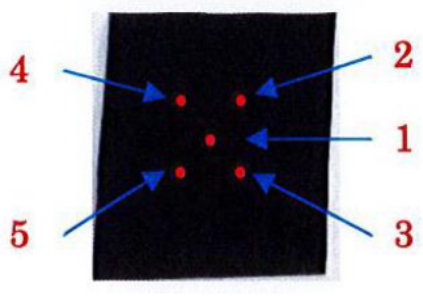

Fig.2.4 Images of 5 test points in thermal diffusivity measurement.

2.2.3.4 High temperature and humidity test

To evaluate the long-term performance of CNF sheets under extreme condition, the high temperature and humidity test was also measured. The experiment device and the place method are showed in Fig. 2.5. The size of samples is 20mm×20mm. The sample under a net was place on a petri dish. The experimental conditions were set up as: temperature was 358K, relative humidity (RH) was 85% and holding time was 500 hours.

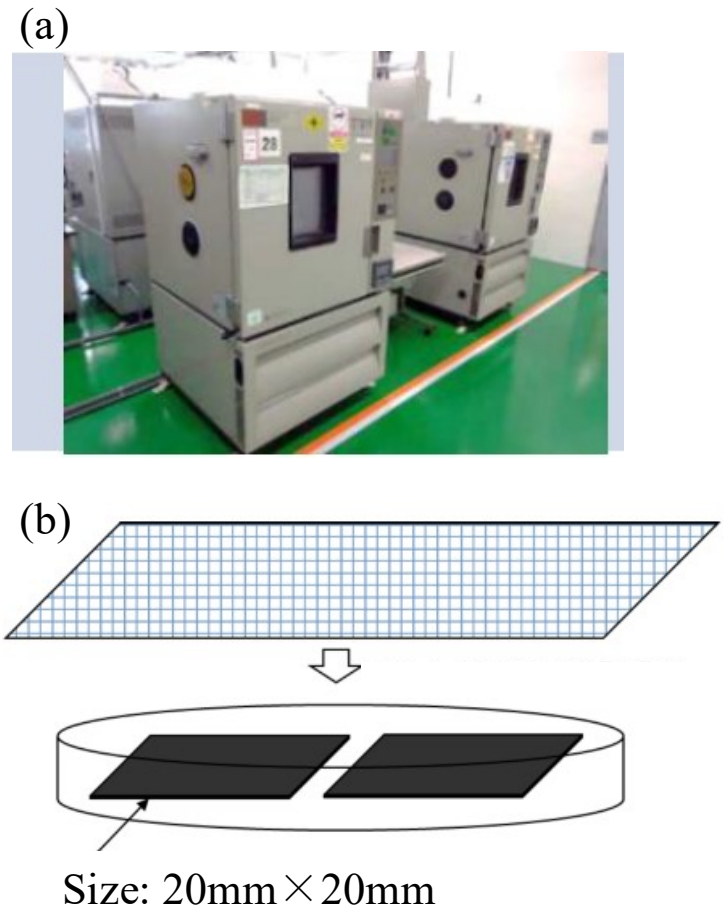

Fig. 2.5 Image of (a)experimental device of high temperature and humidity test, (b) place method of samples.

2.3 Results and discussion

2.3.1 Microstructures and porosity of PVA-VGCF sheet

Fig. 2.6 and Fig. 2.7 shows the photograph and SEM images of the PVA-VGCF sheets. The fabricated sheet was soft and flexible with two surfaces: upper surface and bottom surface, due to the difference in the contact condition. The upper surface was contact with air. Fig. 2.6 (a)~(e) show the SEM images of the upper surface microstructure by different mass ratio of PVA:VGCF (1:0.100, 1:0.070, 1:0.050, 1:0.030, 1:0.025). All of sheets was shown that VGCFs were arranged in random directions and connected with each other via PVA aggregates. In Fig. 2.6(a), a lot of pores were observed between VGCFs. At the PVA:VGCF ratio of 1:0.100, due to the relatively low ratio of PVA, PVA can neither effectively infiltrate the VGCFs nor construct a uniform surface; thus, there were a large number of obvious pores exhibit in surface of PVA-VGCF sheet. As shown in Fig. 2.6(b) ~ (e), with the reduction of VGCF ratio and the increasement of PVA ratio, the pore between VGCFs has been filled by PVA and the porosity of fabricated sheet was decreased. Porosity of each PVA-VGCF sheets was calculated by using image analysis software Image Pro, the result is shown in Fig. 2.8. The porosity of the 5 types of PVA-VGCF sheets decreases from 25% to 22%, 18%, 17%, 13%, by decreasing the amount of VGCFs, which was considered due to the numbers of intersection between VGCFs. Decreasing the amount of VGCFs would also decrease the intersections between VGCFs. Because of these intersections, the PVA-VGCF sheets obtained a cellulose-like structure, through which the PVA infiltration between VGCFs was hindered during the mixing process, thereby leading to pore formation in the fabricated sheet. Therefore, decreasing the amount of VGCFs lead to a lower porosity in CNF sheet. Fig. 2.7 showed the SEM images of bottom surface of fabricated CNF sheets. The bottom surface was in contact with PET film holder which was relatively flat and had a lower surface roughness. For the same reason, due to the low content of PVA, Fig. 2.7 (a) showed a lot of large pores existed in the microstructure of fabricated sheet. As shown in Fig. 2.7(b) ~ (e), with the reduction of

VGCF ratio and the increasement of PVA ratio, the pore between VGCFs has been totally filled by PVA.

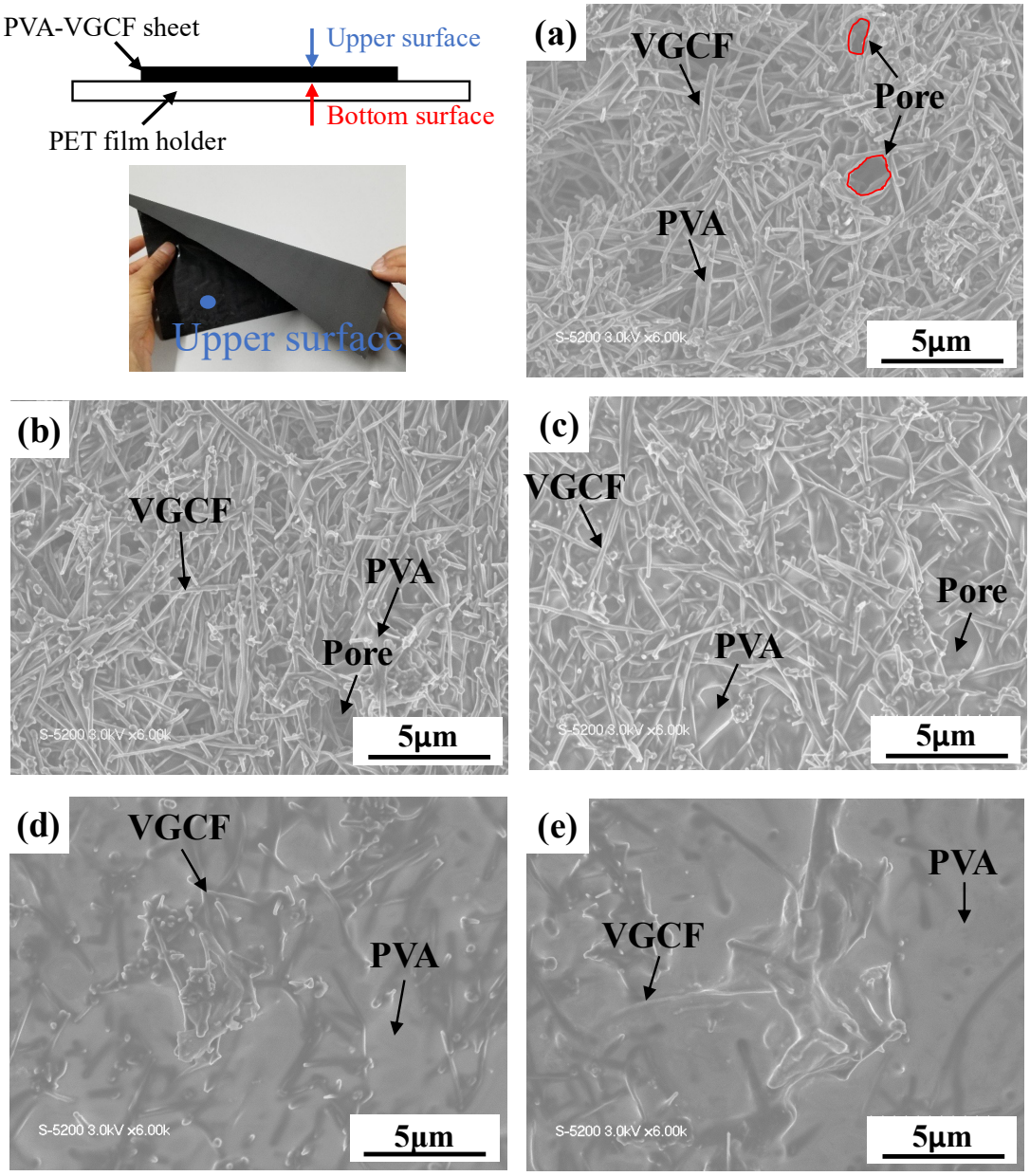

Fig. 2.6 SEM images of upper surface of fabricated CNF sheets by different mass ratio of PVA : VGCF, (a)1 : 0.100, (b)1 : 0.070, (c)1 : 0.050, (d)1 : 0.030, (e)1 : 0.025.

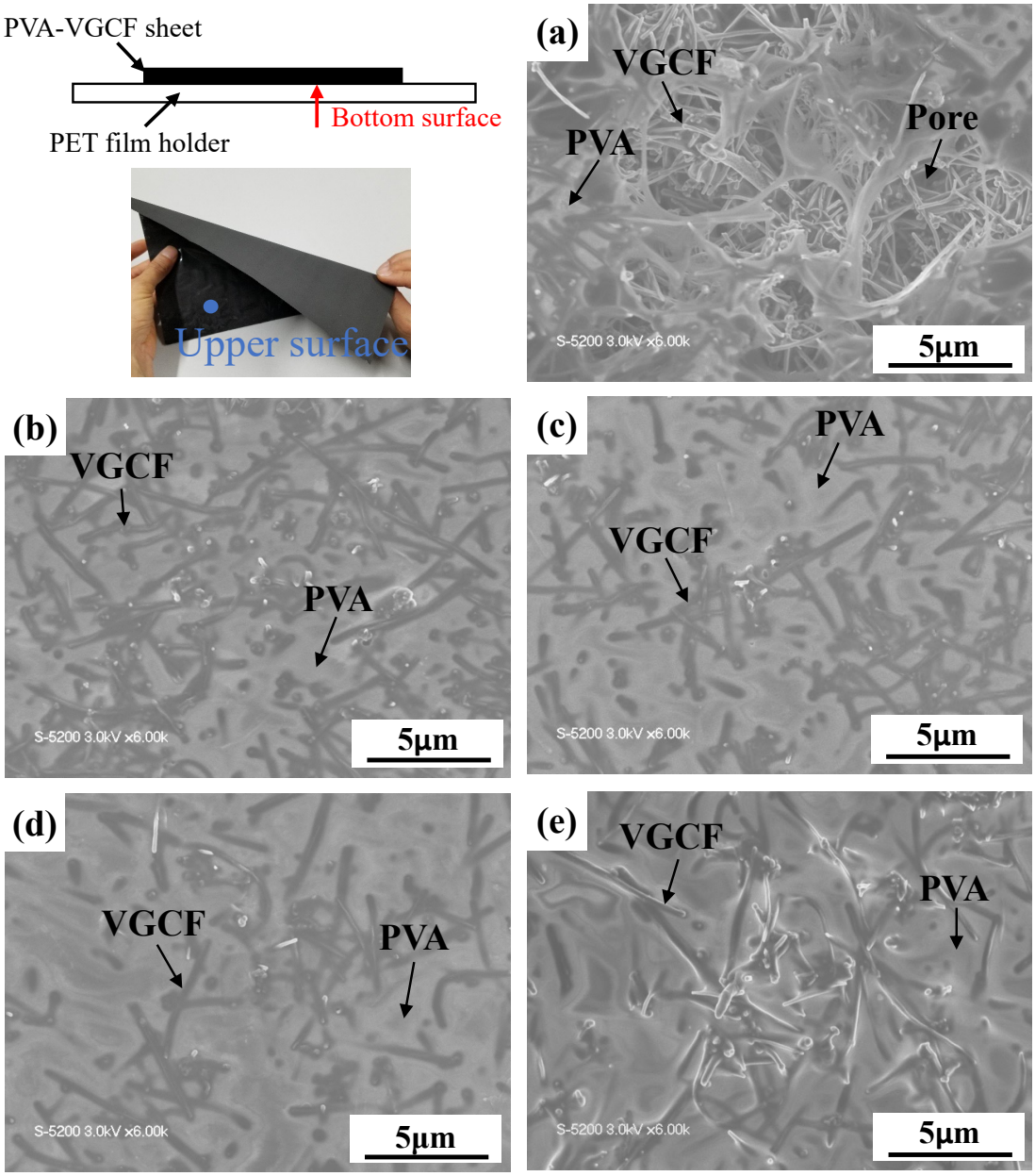

Fig. 2.7 SEM images of bottom surface of fabricated CNF sheets by different mass ratio of PVA : VGCF, (a)1 : 0.100, (b)1 : 0.070, (c)1 : 0.050, (d)1 : 0.030, (e)1 : 0.025.

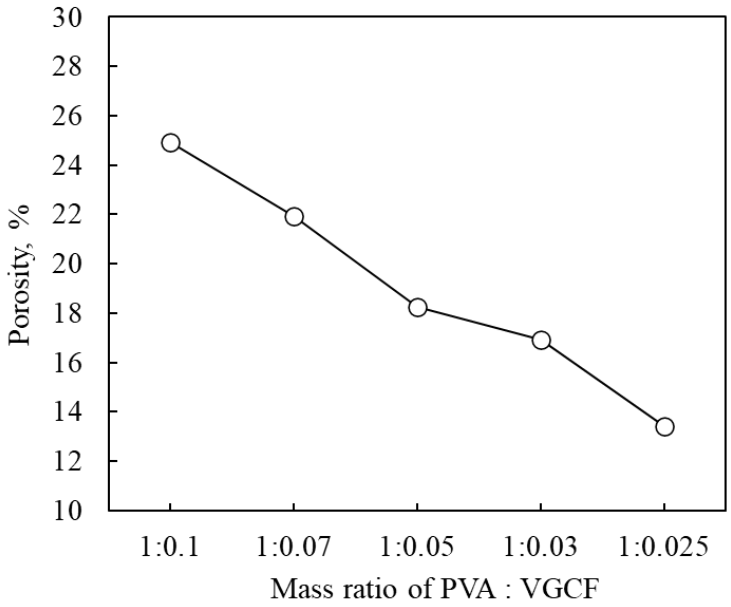

Fig. 2.8 Effect of mass ratio of PVA:VGCF on porosity.

2.3.2 Thickness, density and Shore hardness of PVA-VGCF sheet

In order to evaluate the possibility of the fabricated PVA-VGCF sheets for practical TIM application, thickness, density and Shore hardness of PVA-VGCF sheets were measured. Fig. 2.9 shows the relationship between thickness and density by amount ratio of VGCF and PVA. Average thickness of each PVA-VGCF sheet was 56, 52, 47, 35 and 30μm, it was showed that the fabricated sheets are become thicker by decreasing amount of VGCFs. Considering the flat and smooth surface between semiconductor and heat sink, it is better to keep the thickness of TIM to be about 0.5mm or less. It should be noted that the air gaps between the semiconductor and heat sink could not be effectively filled in wafer-thin TIMs. The thickness of sheet b (PVA:VGCF=1: 0.07) and sheet c (PVA:VGCF=:0.05), which was 52μm and 47μm, were thought to be the ideal thickness for TIM, because the thinner TIM could not to fill air gaps effectively and the thicker TIM would increase the thermal resistance between semiconductor and heat sink. The density of each PVA-VGCF sheet was calculated by mass and volume, the results was $1.10\times10^{6}g\cdot m^{-3}$, $1.06\times10^{6}g\cdot m^{-3}$, $1.03\times10^{6}g\cdot m^{-3}$, $1.15\times10^{6}g\cdot m^{-3}$, $1.12\times10^{6}g\cdot m^{-3}$. It was found that the fabricated sheets keep a relative constant density, although fabricated by different mass ratio of PVA and VGCF and the density results showed the lightweight property of PVA-VGCF sheets compared to some commercially available TIMs ($1.44 \sim 3.6 \times 10^{6}$ $g\cdot m^{-3}$)[12]. In hardness test, according to ASTM D2240 procedure, each PVA-VGCF sheet was superimposed into the same thickness (6mm) and measured by Shore hardness. The result is shown in Fig. 2.10. The hardness of each PVA-VGCF sheet was 83.4HS, 84.4HS, 82.2HS, 83.6HS, 83.8HS. There was not obvious difference between fabricated sheets in Shore hardness, a constant hardness was thought to be obtained successfully. It is interesting that the fabricated sheets obtained a similar Shore hardness to that of commercial soft lining material[13], it was implied the great softness and flexibility of fabricated PVA-VGCF sheets for practical application of TIM.

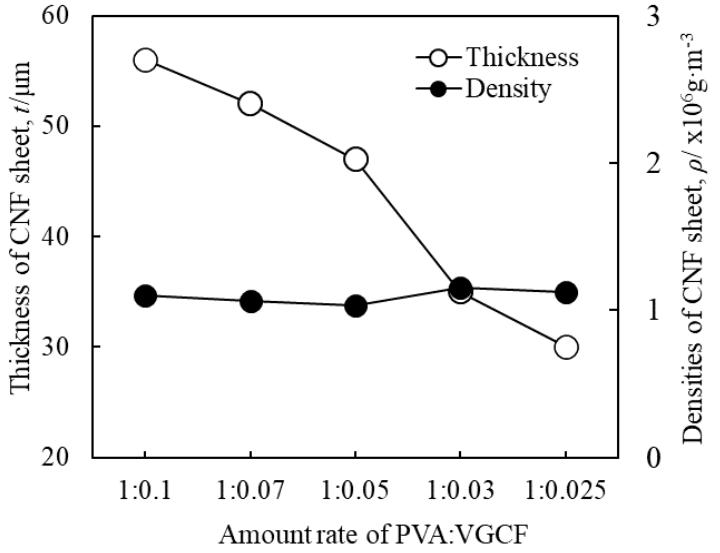

Fig. 2.9 Effect of mass ratio of PVA:VGCF on the thickness and density of fabricated sheets.

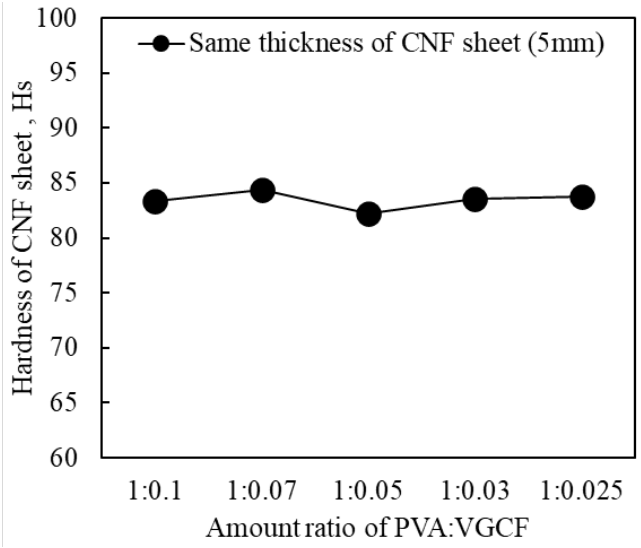

Fig. 2.10 Hardness of fabricated PVA-VGCF sheets by different mass ratio of PVA:CNF.

2.3.3 Thermal properties of PVA-VGCF sheet

Fig. 2.11 and Fig. 2.12 shows the effect of mass ratio of PVA and VGCF on in-plane and through-plane thermal conductivities of PVA-VGCF sheet, respectively. As we known, the pure PVA resin has low thermal conductivity of about 0.28 $W \cdot m^{-1} \cdot K^{-1}$, and VGCF used in this study has a high thermal conductivity of 1200.00 $W \cdot m^{-1} \cdot K^{-1}$ at room temperature[14]. As shown in Fig.2.11, the PVA-VGCF sheets were fabricated by amount of VGCFs: 1:0.1(17.04 vol.%), 1:0.07(12.85 vol.%), 1: 0.05 (10.15 vol.%), 1: 0.03 (8.18 vol.%), 1: 0.025 (7.95 vol. %), and the corresponding in-plane thermal conductivity was shown as 3.40, 1.34, 6.44, 3.25 and 1.51 $W \cdot m^{-1} \cdot K^{-1}$, and though-plane thermal conductivity was obtained as 12.94, 8.87, 14.30, 8.90, and 5.29 $W \cdot m^{-1} \cdot K^{-1}$, respectively. Among all fabricated sheets, PVA-VGCF sheet c had the max thermal conductivities as 6.44 $W \cdot m^{-1} \cdot K^{-1}$ in plane and 14.30 $W \cdot m^{-1} \cdot K^{-1}$ throughout plane. Moreover, both of in-plane and through-plane thermal conductivities showed a non-linear relationship with different VGCF content, it can be suggested that the thermal conductivity was not only influenced by amount of VGCFs. Although VGCF was used as thermally conductive material in this study, as mentioned above, the porosity of fabricated sheet would also increase by increasing the amount of VGCF. The pores in fabricated sheet were like air gaps, will decrease thermal properties apparently and cause a low density. This was the reason why sheet a and sheet b appeared lower thermal conductivities. Moreover, overloading of VGCFs may also result in a deterioration of mechanical properties of PVA-VGCF sheet. Therefore, minimizing the amount of VGCFs while keeping high thermal properties is preferable for sheet fabrication[15]. In addition, there was a large thermal conductivity error of sheet a as shown in Fig. 2.12, it was also caused by the high porosity. Because the thermophysical properties of the fabricated sheets were measured using periodical heating radiation-temperature measuring method in this study, the laser diameter was 100 ~ 150μm, which means the result was easily affected by the surface condition and roughness of sample. Meanwhile, due to the high porosity of sheet a, a large number of pores can readily structure an undulating surface. Considering the thickness of sheet a was only 56μm, some large pores shown in Fig. 2.6(a) would also lead to an obvious reduction of thickness in this

area. The undulating surface and uneven thickness of sheet a can have a strong influence on heat radiation and the calculation of thermal conductivity. Therefore, there was a large thermal conductivity error of PVA-VGCF sheet a. As for PVA-VGCF sheet d and sheet e, the low thermal conductivity was caused by low VGCF content, and the irregularity of surface which has mentioned above. Table 2.2 lists previously reported thermal conductivity of other polymer-based carbon TIMs. As shown in this table, the through-plane thermal conductivity of CNF sheet in this study is significantly higher than those of previous studies. Although the in-plane thermal conductivity of CNF sheet is not the best, but it is still higher than the most of reported thermally conductive materials. By using a simple and cost-effective process, the integration of high thermal conductivity, lightweight and super flexibility makes the CNF sheets highly promising for heat management of advanced electronic device.

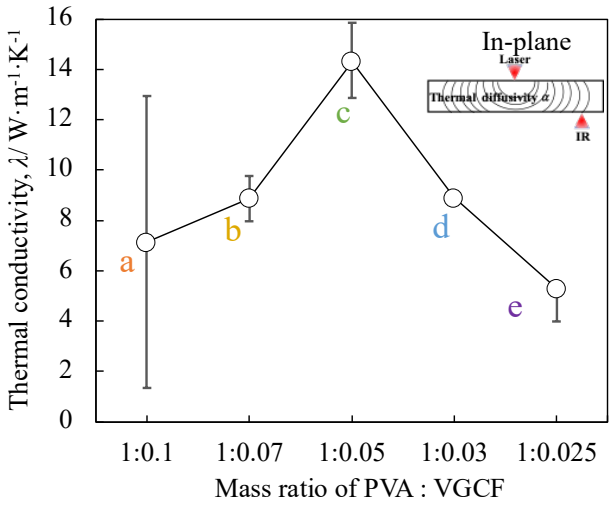

Fig. 2.11 Effect of mass ratio of PVA and CNF on the in-plane thermal conductivity.

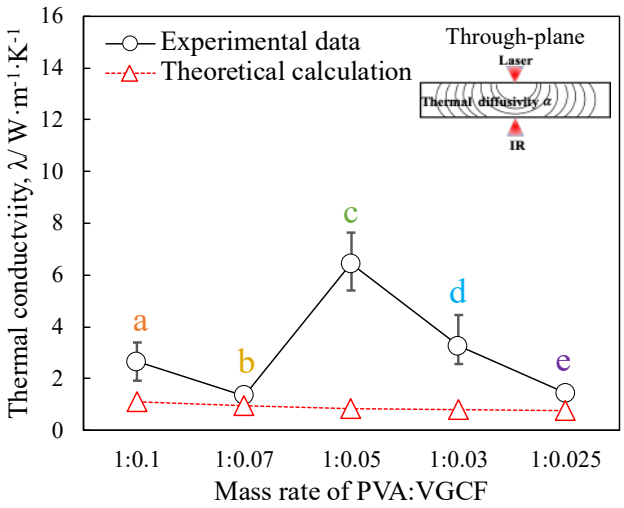

Fig. 2.12 Effect of mass ratio of PVA and CNF on the through-plane thermal conductivity.

Table 2.2 Comparison of thermal conductivity of our PVA-VGCF sheet with other polymer-based carbon TIMs.

Material	Matrix	Fraction	Thickness [t/μm]	Thermal conductivity [λ/W·m^{-1}·K^{-1}]		Reference
				In-plane	Through-plane	
CNF	PVA	10.15 vol%	47	14.30	6.44	This study
3D-Carbon fibers network	Epoxy	13 vol%	Unknown	1.70	2.84	16
CNT	Epoxy	16.7 vol%	Unknown	1.00	4.87	17
Graphite nanoplatelet	PVDF	2.5 wt%	50	Unknown	0.72	9
Graphene aerogel	Epoxy	0.92 vol%	Unknown	0.63	2.13	18
Templated graphene framework	Epoxy	8.3 wt%	Unknown	8.80	2.00	19
Graphene nanoplatelet	Nature rubber	27.48 vol%	71	39.27	1.50	20

2.3.4 High temperature and humidity test results

In this chapter, the PVA-VGCF sheet (PVA:VGCF=1:0.050), which had the highest value of thermal conductivities among the fabricated sheets, was cut into 4 specimens with a size of 20×20mm for high temperature and humidity test. Each specimen was held at the temperature of 358K and relative humidity (RH) of 85% for 500 hours. After the high temperature and humidity test, the average of in-plane and through-plane thermal conductivity of 4 specimens was measured. As shown in Fig. 2.13 and Fig. 2.14, it was indicated that before test the in-plane thermal conductivity had a high value as 14.30 $W \cdot m^{-1} \cdot K^{-1}$, but after test the average in-plane thermal conductivity of 4 specimens decreased to 9.85 $W \cdot m^{-1} \cdot K^{-1}$, with a reduction of 31%. As the same, before test the through-plane thermal conductivity was 6.44 $W \cdot m^{-1} \cdot K^{-1}$, and after test the average through-plane thermal conductivity decreased to 2.71 $W \cdot m^{-1} \cdot K^{-1}$, which was reduced by nearly 57%. It was considered that the reduction of thermal conductivity was caused by the hydrophilic property of PVA. The water in PVA increased porosity and decreased thermal properties of fabricated sheet. The water molecules in the environment would be absorbed into fabricated sheets by PVA. The absorbed water in PVA not only disrupts hydrogen bonding, but also contributes more free volume and lubrication. The PVA segments in fabricated sheets become readily mobile and rapidly responding to the load change[21], which may lead to a movement of PVA from surface to center part of PVA-VGCF sheet. A large number of pores would be generated in surface of fabricated sheet. Therefore, absorbed water in PVA increased the porosity and degraded the thermal properties of the PVA-VGCF sheets.

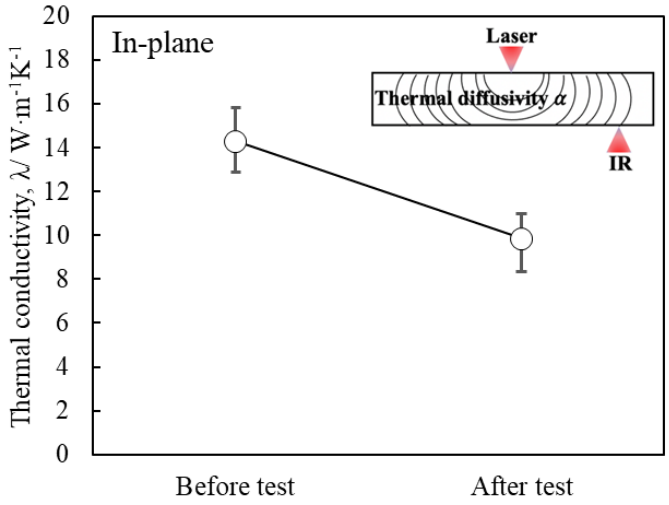

Fig. 2.13 In-plane thermal conductivity of specimens before and after the high temperature and humidity test.

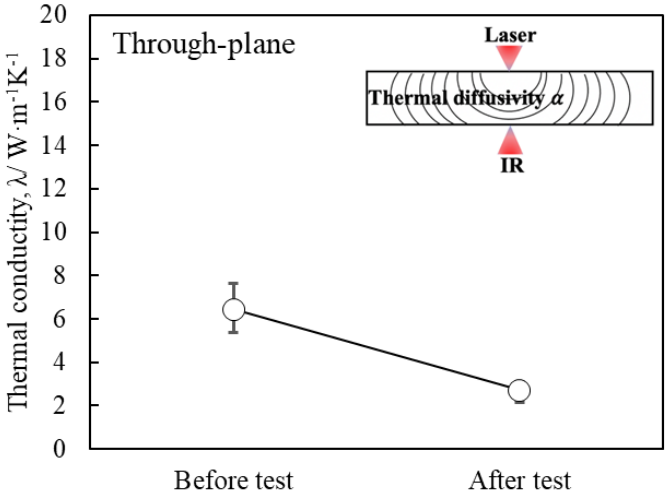

Fig. 2.14 Through-plane thermal conductivity of specimens before and after the high temperature and humidity test.

2.4 Summary

In this chapter, an innovative thermal interface material based on a composite of PVA and VGCF was fabricated successfully, by a simple and cost-efficient procession method. 5 kind of CNF sheets have been fabricated with different mass ratio of PVA:VGCF, the in-plane and through-plane thermal conductivities were measured. The mechanical properties of each CNF sheet also have been tested. From this work, the important results are list below:

(1) The VGCFs in fabricated sheets were arranged in random directions and connected with each other via PVA aggregates. A lot of pores existed between VGCFs due to the evaporation of water. The porosity of CNF sheets decreased by decreasing the amount of VGCF.

(2) The thickness of CNF sheets increased by increasing the amount of VGCF. The density and hardness of CNF sheets had not apparent difference between each fabricated sheet.

(3) The highest value of thermal conductivity was 6.44 $W \cdot m^{-1} \cdot K^{-1}$ in-plane and 14.30 $W \cdot m^{-1} \cdot K^{-1}$ through-plane. Reducing the amount of VGCF would decrease the thermal conductivity apparently. However, increasing the amount of VGCF excessively could also bring an increase of porosity in CNF sheet and reducing the thermal conductivity.

(4) The in-plane and through-plane thermal conductivities had obvious reductions after the high temperature and humidity test due to the hydrophilic property of PVA.

References

[1] Y. L. Ji, H. L.Yan, X. Xiao, J, T. Xu, Y, T. Li, C. Chang: Appl. Therml. Eng. **166** (2020) 114649.

[2] J. W. Zhao, R. Zhao, Y. K. Huo, W. L. Cheng: Int. J. Heat Mass Transf. **140** (2019) 705-716.

[3] Y.C. Li, G. L. Sang, H. W. Shi: J. New Mater. Electrochem. Syst. **17** (2014) 123-127.

[4] Y. X. Fu, Z. X. He, D. C. Mo, S. S. Lu: Int J Therm Sci. **86** (2014) 276-283.

[5] L. Peng, Z. Xu, Z. Liu: Advanced Material **29** (2017) 1700589.

[6] H.Y Sun et al.: Chem. Mater. **29** (2017) 7808-7815.

[7] J. Khan, S. A. Momin, M. Mariatti: Carbon **168** (2022) 65-112.

[8] Y. Gogotsi: Nanotubes and Nanofibers (CRC Press, New York, 2006) pp. 51-58.

[9] Q. S. Song, W. Zhu, Y. Deng, D. L. He, J. J. Feng: Compos. Sci. Technol. **168** (2018) 381-387.

[10] N. D. Greef, L. X. Zhang, A. Magrez, L. Forró, J. P. Locquet, I. Verpoest, J. W. Seo: Diam Relat Mater. **51** (2015) 39-48.

[11] W. T. Hong, N. H. Tai: Diamond Relat. Materi. **17** (2008) 1577-1581.

[12] C. P. Feng: Compos. Commun. **22** (2020) 100528.

[13] I. M. Meththananda, S. Parker, M. P. Patel, M. Braden: Dent. Mater. **25** (2009) 956-958.

[14] Y. M. Et al.: J. Mater. Chem. C. **24** (2018) 6469-6501.

[15] H. F. Song et al.: Joule **2** (2018) 442-463.

[16] J. K. Ma et al.: Chem. Eng. J. **380** (2020) 122550.

[17] A. Marconnet, N. Yamamoto, M. A. Panzer, B. L. Wardle: ACS Nano **5** (2011) 4818-4825.

[18] G. Lian et al.: Chem. Mater. **28** (2016) 6069-6104.

[19] X. Shen et al.: Mater. Horizons **5** (2018) 275-284.

[20] C. P. Feng et al: Compos. Commun. **12** (2019) 80-85.

[21] R. M. Hodge, T. J. Bastow, G. H. Edward, G. P. Simon, A. J. Hill: Macromolecules **29** (1996) 8137-8143.

Chapter 3

Effects of polytetrafluoroethylene addition on microstructure and thermal properties of PVA-VGCF sheet

3.1 Introduction

The thermal interface materials (TIMs) are used to fill the air gaps between a heat-generation device and a heat-dissipation thrust for heat distribution. With the rapid development of the electronics industry, the rising higher power density in electronics presents an increasing requirement for heat dissipation, because electronics are becoming intelligent, miniaturized, and integrated. Thus, the development of TIMs become extremely significant for the heat management of advanced electronic products. Besides of thermal properties, the functional property of TIM is also required now. For example, for electronic equipment used in scientific research experiments in Antarctica, its TIMs need to endure the minimum temperature to 183K[1] and maintain a certain degree of flexibility and thermal conduction ability. For the electronic equipment used in Amazon rainforest with a flexible environment of a relative humidity high at an average of 88% in the rainy season and 77% in the dry season[2], TIMs used in this region require a higher humidity resistance than usual.

In chapter 2, we reported an efficient and simple method to fabricate polyvinyl alcohol (PVA)-based VGCF sheet with a mass ratio of VGCF:PVA = 1:2.6, which high TC of 6.44 $W \cdot m^{-1} \cdot K^{-1}$ in the through-plane direction and 14.30 $W \cdot m^{-1} \cdot K^{-1}$ in the in-plane direction. The PVA-based VGCF sheet also has a lightweight property with a density of 1.03×10^6 $g \cdot m^{-3}$ and is as soft as commercial soft lining materials with a Shore hardness of 82.2HS. However, the thermal conductivities were significantly reduced after the high temperature and humidity test, due to the hydrophilic property of PVA. Polytetrafluoroethylene(PTFE) consisting of carbon and fluorine, has excellent hydrophobicity and good dispersibility, and high chemical stability[3,4], which is considered to be an excellent filler to enhance the hydrophobicity of composite material for practical application. Moreover, dispersed nanometric scale reinforcement significantly increases the tortuosity of the path for the permeation of water molecules. However, it should be noted that excessive addition of PTFE powders would significantly reduce the thermal conductivities of the fabricated sheet, due to the low

TC of PTFE (~0.3 $W \cdot m^{-1} \cdot K^{-1}$). Considering all the above, it is believed that the hydrophobicity of the PVA-VGCF sheet will be enhanced by adding PTFE nano powders, while keeping the mass ratio of VGCF : resin (PVA and PTFE) the same as that of previous PVA-VGCF sheet.

This chapter has focused on understanding the full influence of the use of an optimized mass ratio of PTFE (VGCF:PVA:PTFE=1:1.3:1.3) as a filler in the VGCF sheet, for guaranteeing an improvement in hydrophilicity. All the experimental results of the VGCF:PVA:PTFE sheet were compared with the PVA-VGCF sheet of the previous report to evaluate the influence of added PTFE powders on their properties.

3.2 Experimental procedure

3.2.1 Raw materials

The VGCFs were purchased from SHOWA DENKO K.K. and have an excellent thermal conductivity of 1200 $W \cdot m^{-1} \cdot K^{-1}$ and a length of 10 - 20 μm. Commercial PVA (Yamato Co., Ltd.) with a concentration of 13 mass% was used as a binder. As showed in Fig. 3.1, two types of PTFE particles with different size: L173JE(120nm) and TF9207Z(300nm) were used to improve the hydrophobicity of the PVA-VGCF sheet, which were supplied by 3M Japan Ltd., and AGC Chemical Company, respectively.

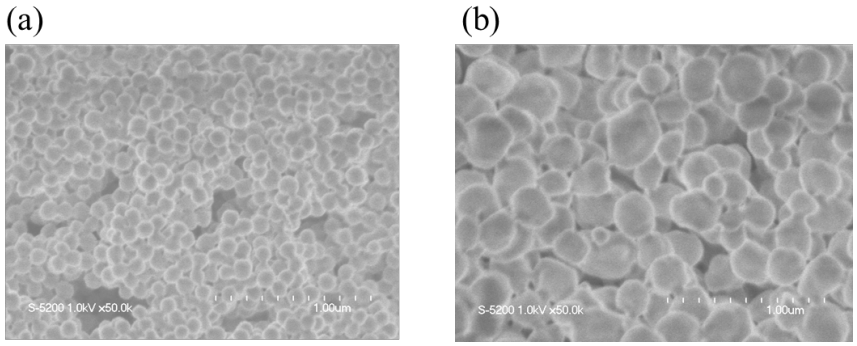

Fig. 3.1 FE-SEM image(×6000) of: (a)PTFE powders of 120nm and (b)PTFE powders of 300nm.

3.2.2 Fabrication method of PVA-PTFE-VGCF sheet

The preparation process of the PVA-PTFE-VGCF sheet is shown in Fig. 3.2. Based on solution mixing, a simple but industrial method was adopted to fabricate the VGCF sheet. To make PTFE powders dispersed evenly in a fabricated sheet, PTFE powders were mixed PVA binder by an agitator at 100 rpm for 1 hour. After that, the VGCFs were poured into the PVA-PTFE mixture and mixed with a silicon bar at 20 rpm for 1 minute, the PVA-PTFE-VGCF mixture was spread on a PTFE film of A4 paper size. At last, after drying this at room temperature (RT) for 48 hours, the PVA-PTFE-VGCF sheet was separated from the PTFE film. In this study, two types of PVA-PTFE-VGCF sheets: PVA-PTFE L173JE-VGCF sheet (PPLV) and PVA-PTFE TF9207Z-VGCF sheet (PPTV) were fabricated by using different PTFE particles of L173JE (120nm) and TF9207Z (300nm). The fabrication condition is listed in table 3.1.

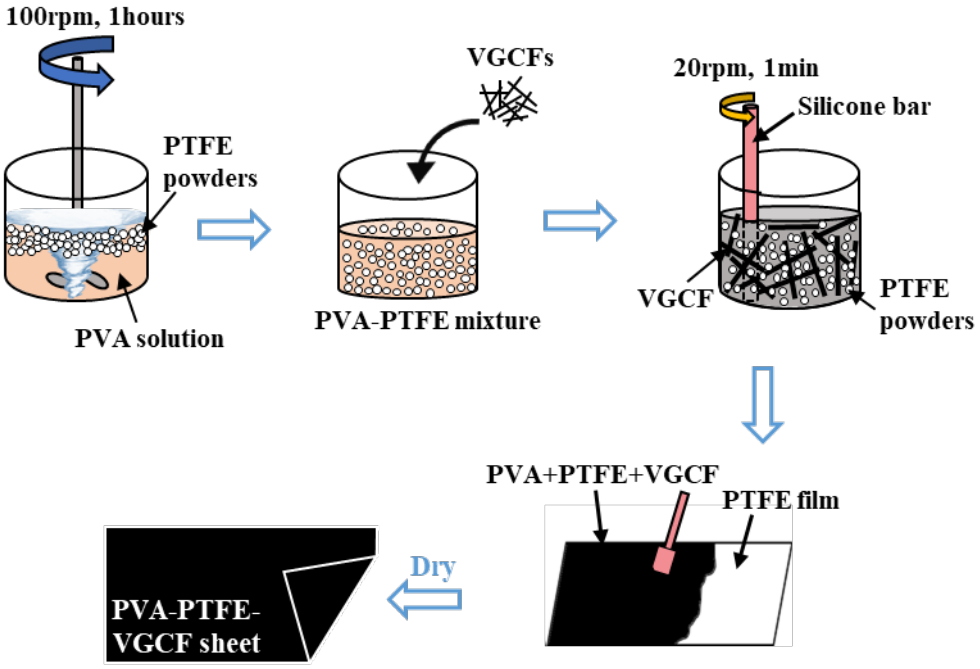

Fig. 3.2 Schematic of the fabrication procedure of PVA-PTFE-VGCF sheet.

Table 3.1 Fabrication conditions of PVA-PTFE-VGCF sheets.

Samples	VGCF:PVA:PTFE (mass%)	Particle size of PTFE (nm)	VGCF (mass%)
PPLV	1:1.3:1.3	120	27.78%
PPTV	1:1.3:1.3	300	

3.2.3 Evaluation method and equipment

The dispersion of PTFE powders in the PVA matrix and the morphology of fabricated sheets were checked by FE-SEM. The porosity of each VGCF sheet was calculated by using the image analysis software Image-Pro Plus 6.0, which used five random areas with a size of 1.28×10^{-3} mm^2 from each VGCF sheet. The thickness of fabricated sheets was measured by using a digital micrometer (MonotaRo Co., Ltd.). Density was calculated from the mass and volume of each fabricated VGCF sheet. According to the ASTM D2240 procedure[5], the fabricated VGCF sheets with a total thickness of 6 mm were used for the Shore hardness test by using a Shore hardness durometer. The thermal diffusivity (α) of fabricated sheets at RT was evaluated using a periodic heating and infrared radiation thermometer method (Thermowave Analyzer TA). Specific heat capacity (*Cp*) was measured by using DSC (X-DSC 7000, HITACHI, Japan). After getting all these values, TC was calculated by equation (2.1). To evaluate the long-term performance of the fabricated sheets, the high temperature, and humidity test was performed at a temperature of 358K and relative humidity (RH) of 85% for 500 hours. The infrared spectra of the fabricated PVA-PTFE-VGCF sheet were measured by using a Fourier transform infrared spectrometer (FT-IR) in the range of 4000 cm^{-1} to 600 cm^{-1}. FT-IR is a technique that is used to obtain infrared spectrum of absorption, emission and photoconductivity of solid, liquid and gas[6], which is often used to identify organic and polymeric materials.

3.3 Results and discussions

3.3.1 Microstructures of PVA-PTFE-VGCF sheet

Fig. 3.3 shows the SEM images and microstructure schematics of referred PVA-VGCF sheets and fabricated PVA-PTFE-VGCF sheets. All of the sheets were shown that VGCFs were arranged in random directions and connected with each other via PVA aggregates. Because of the aggregation of as-received VGCFs, a 3D net-like structure was built by VGCFs, which contribute high through-plane TC and good physical stability to fabricated sheets. On the other hand, as shown in Fig3.3 (a), the intersections of the 3D network structure also led to the difficulty for PVA to enter inside during mixing and created many pores in the reference PVA-VGCF sheet, resulting in a significant decrease in TC. In Fig. 3.3(b) and 3(c), the microstructures showed that the addition of PTFE powder can effectively filled these pores. However, partial aggregation of PTFE particles was also observed due to the intermolecular forces of PTFE particles. Especially for 120nm PTFE, some large collections of 120nm PTFE particles and unfilled pores were observed in Fig. 3.3(b). This poor dispersion of 120nm PTFE powder will adversely affect the efficiency of heat dissipation in the fabricated sheet. On the contrary, it can be clearly seen from Fig. 3.3(c) that the 300nm PTFE particles were still well distributed and compatible in the fabricated PPTV sheet due to the smaller aggregates, and the pores between VGCFs were almost filled by 300nm PTFE particles. Furthermore, the schematic diagram of the microstructure showed that the different dispersion of 120nm and 300nm PTFE powders leads to different microstructures in the fabricated sheets. Smaller PTFE particles were more likely to aggregate and form uneven surfaces, while 300 nm PTFE particles can be relatively uniformly dispersed among VGCFs and filled the pores effectively.

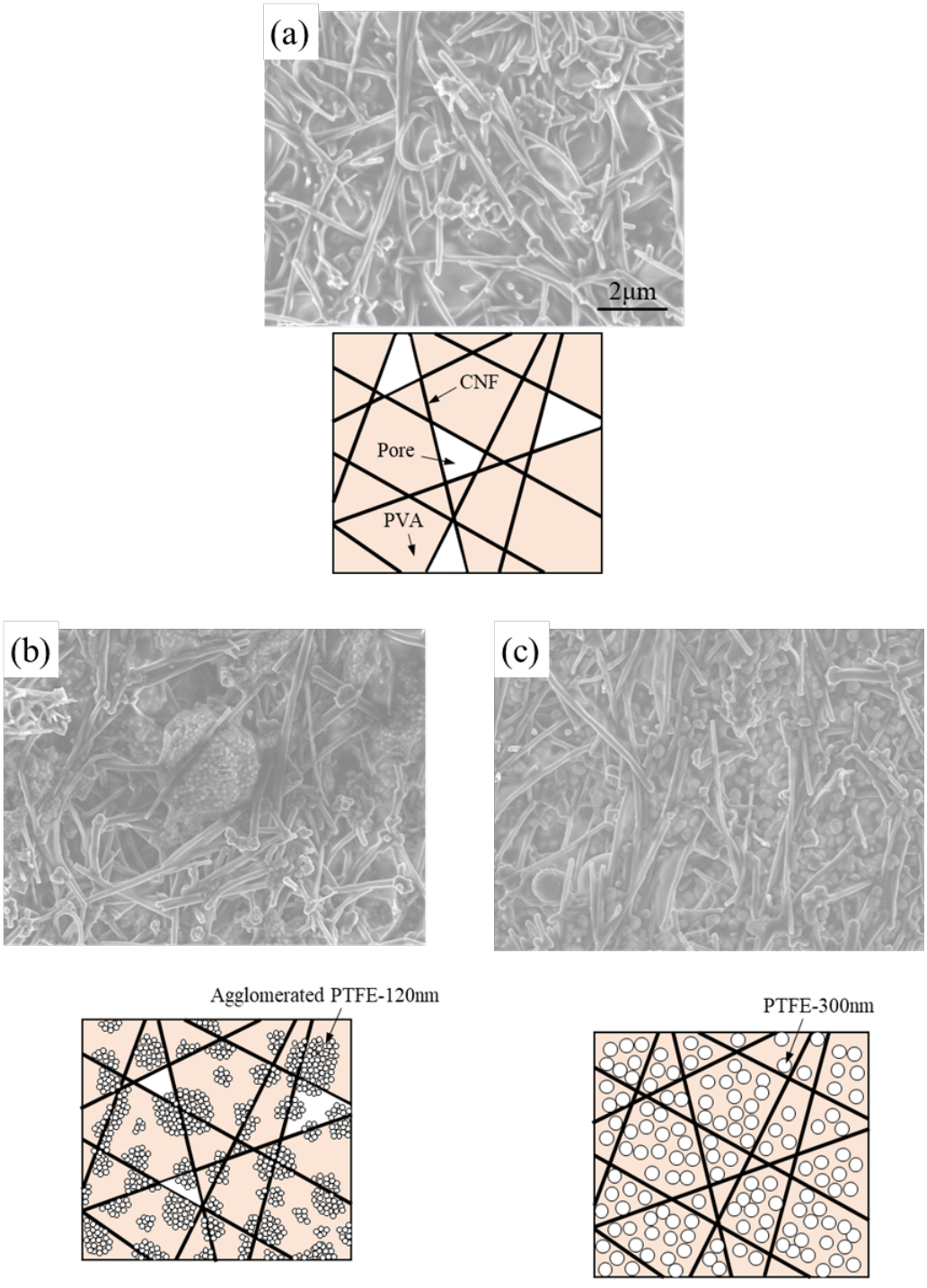

Fig. 3.3 SEM images (×6000) and microstructure schematics of fabricated VGCF sheets: (a) PVA-VGCF sheet*, (b) PPLV sheet and (c) PPTV sheet.

3.3.2 Porosity, Thickness, density and hardness of PVA-PTFE-VGCF sheet

To evaluate the possibility of a fabricated VGCF sheet for practical application for TIM, the porosity, thickness, density, and Shore hardness was measured. As shown in Fig. 3.4, the porosity of the reference PVA-VGCF sheet was as high as 18%. After adding PTFE particles, although the concentration of PVA decreased, which means more pores should be produced theoretically[7], the porosity of PPLV sheet and PPTV sheet are reduced to 9% and 6% respectively due to the pores were filled by PTFE particles. And due to the aggregation of 120nm PTFE particles, the porosity of PPLV sheet was higher than that of PPTV sheet.

As the same, the average thickness of the VGCF sheet was also decreased from 47μm for the PVA-VGCF sheet to 31.2μm and 28.2μm for PPLV and PPTV sheets respectively, due to the lower content of the PVA matrix. It is considered that agglomeration of 120nm PTFE particles were much larger than that of 300nm PTFE particles and cannot fill the pores of fabricated VGCF sheets. Agglomeration of 120nm PTFE particles caused surface unevenness and increased the thickness of the fabricated sheet. In addition, the thickness of TIM has a great influence on the absolute thermal resistance across the TIM. From Fourier's Law for heat conduction, the absolute thermal resistance R_θ of TIM is calculated by using the equation:18):

$$R_\theta = \frac{t}{A \times \lambda} \tag{3.1}$$

where t is the thickness of TIM, A is the cross-sectional area perpendicular to the path of heat flow, and λ is the thermal conductivity of TIM. Therefore, the absolute thermal resistance of a TIM will decrease by using thinner material. The lower absolute thermal resistance means this material is a better thermal conductor in practical applications. Therefore, the TIMs with lower thickness such as PPLV and PPTV sheets have greater potential in the application in advanced precision instruments, which have become miniaturized and complex in recent years. However, it should be noted that the air gaps

cannot be efficiently filled in wafer-thin TIMs. In this case, increasing the total mass of PVA, PTFE, and VGCF during the preparation process could increase the thickness of the fabricated VGCF sheet to solve the problem. The density of PPLV and PPTV sheet were calculated using mass and volume, as shown in Fig. 3.5, the values were 0.79×10^{6} $g\cdot m^{-3}$ and 0.91×10^{6} $g\cdot m^{-3}$ respectively. Compared with the PVA-VGCF sheet, PPLV and PPTV sheets had a lower density, which showed a greater lightweight property of PPLA and PPTV sheet compared to some commercially TIMs ($1.44\text{-}3.6\times10^{6}$ $g\cdot m^{-3}$). PPLV and PPTV sheets were superimposed to the same thickness as 6mm to measure their Shore hardness according to ASTM D2240 procedure. The result was shown in Figure 3.5. The average Shore hardness of PVA-VGCF sheet, PPLV and PPTV sheet was 82.2HS, 86.0HS and 85.4HS, respectively. PPLV and PPTV sheets became slightly stiffer than PVA-VGCF sheets due to lower PVA matrix content. Even so, the continuous 3D-net like structure composed of VGCFs allows the fabricated sheets to take advantage of the high elasticity of the PVA matrix to generate large deformation and low stiffness, which suggesting that PPLV and PPTV have great softness and flexibility for practical applications as TIMs.

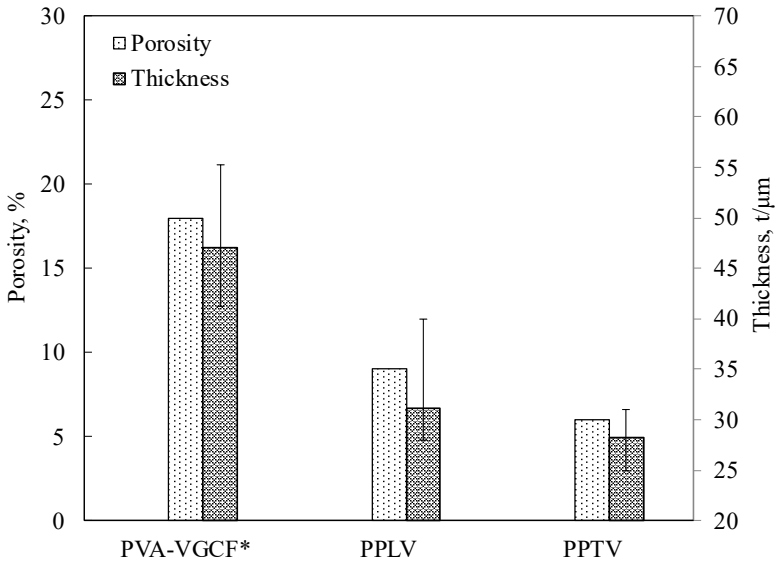

Fig 3.4 The porosity and thickness of fabricated PVA-VGCF*, PPLV and PPTV sheets.

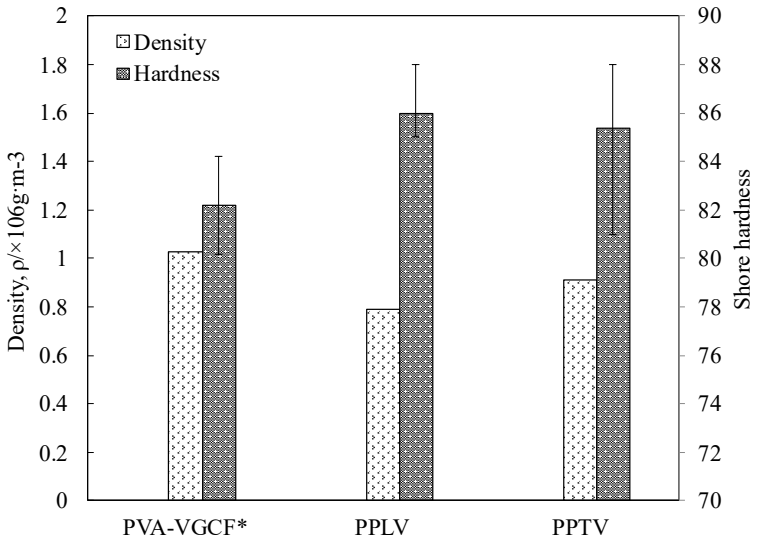

Fig 3.5 The density and shore hardness of fabricated PVA-VGCF*, PPLV and PPTV sheets.

3.3.3 Thermal properties of PVA-PTFE-VGCF sheet

Fig. 3.6 and Fig. 3.7 show the effect of the addition of PTFE powder on the in-plane TC, through-plane TC, and the thermal diffusivities of the fabricated sheets. As shown in Fig. 3.6, with the addition of the PTFE powders, the in-plane TC of PPLV and PPTV sheet had a reduction of 46% and 31% respectively, which decreased from 14.30 $W \cdot m^{-1} \cdot k^{-1}$ to 7.66 $W \cdot m^{-1} \cdot k^{-1}$ of PPLV sheet and 9.81 $W \cdot m^{-1} \cdot k^{-1}$ of PPTV sheet. As shown in Fig. 3.7, the through-plane TC also had a reduction of 72% and 67% after the addition of PTFE powders, which decreased from 6.44 $W \cdot m^{-1} \cdot k^{-1}$ to 1.79 $W \cdot m^{-1} \cdot k^{-1}$ and 2.11 $W \cdot m^{-1} \cdot k^{-1}$, respectively. The thermal diffusivities on the in-plane and through-plane directions of fabricated sheets have similar reduction trends with TC.

In theory, thermal conduction of VGCF, PVA and PTFE is achieved mainly by the vibration of atoms and molecules near their equilibrium position[8]. VGCF has a high TC of 1200.00 $W \cdot m^{-1} \cdot k^{-1}$. On the other hand, due to the low crystallinity of polymer, the PVA and PTFE have very low thermal conductivities, the TC of pure PVA is approximately 0.21 ~ 0.76 $W \cdot m^{-1} \cdot k^{-1}$ and the that of PTFE powders is less than 0.3 $W \cdot m^{-1} \cdot k^{-1}$. Thus, the thermal conduction in PVA-PTFE-VGCF sheet mainly depends on the high thermal conductivity via VGCF networks. The thermal conductive mechanisms in this study include thermal conductive path theory and surface microstructure of fabricated sheet. Through the thermal conductive path theory[9,10], the thermal paths were formed by the contact of VGCFs in the fabricated sheet. The heat flux mainly transferred along the 3D network of VGCF with lower thermal resistance. The PVA and PTFE increased the thermal interface resistance and formed thermal barrier to the thermal paths. This is the first reason for the reduction of TC with the addition of PTFE powders. The surface microstructure was another reason for the reduction of TC, which was shown in Fig. 3.8. Without the filling of PTFE powders, the surface of the PVA-VGCF sheet had a surface wave, which was caused by the bulge of VGCFs. With the addition of PTFE powders, this wave can be filled and reformed into a relatively smooth surface, consisting mostly of PTFE particles and a small part

of bulging VGCFs. When the front surface of the PVA-VGCF sheet was heated by a light pulse, the heat can reach the rear face quickly through the heat paths as shown in Fig. 3.8(a), which is indicated that the PVA-VGCF should have a good thermal diffusivity and TC. As shown in Fig. 3.8(b), due to the low TC of PTFE, adding PTFE powder resulted in forming a thermal barrier, and the heat can only reach the rear face through the small part of bulging VGCFs, which lead to the lower TC of PPLV and PPTV sheet. Table 3.2 lists the previously reported thermal conductivity of other paper-like thermally conductive composites. As shown in this table, the through-plane thermal conductivity of PPLV and PPTV sheet in this study was significantly higher than those of previous studies, while the in-plane thermal conductivity of the fabricated sheet still maintains a higher level among all these paper-like thermally conductive composites.

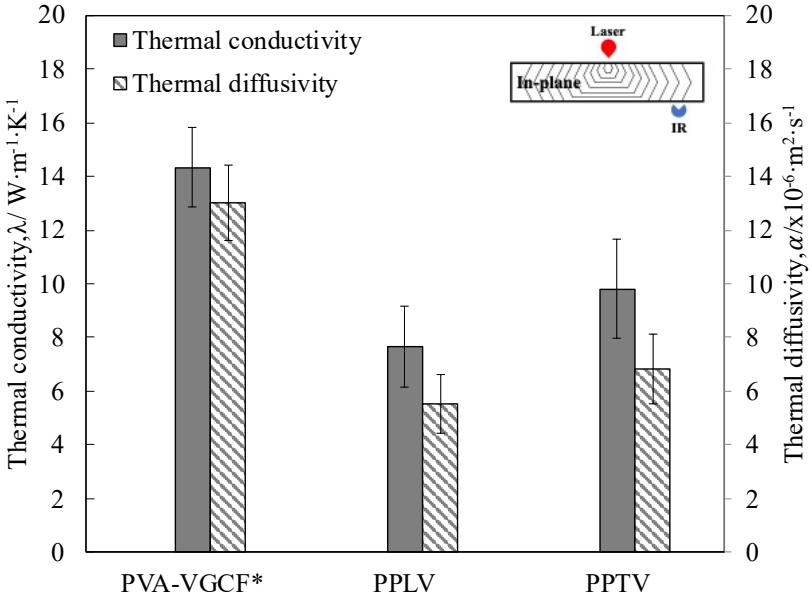

Fig. 3.6 In-plane thermal conductivities and thermal diffusivities of PVA-VGCF, PPLV and PPTV sheet.

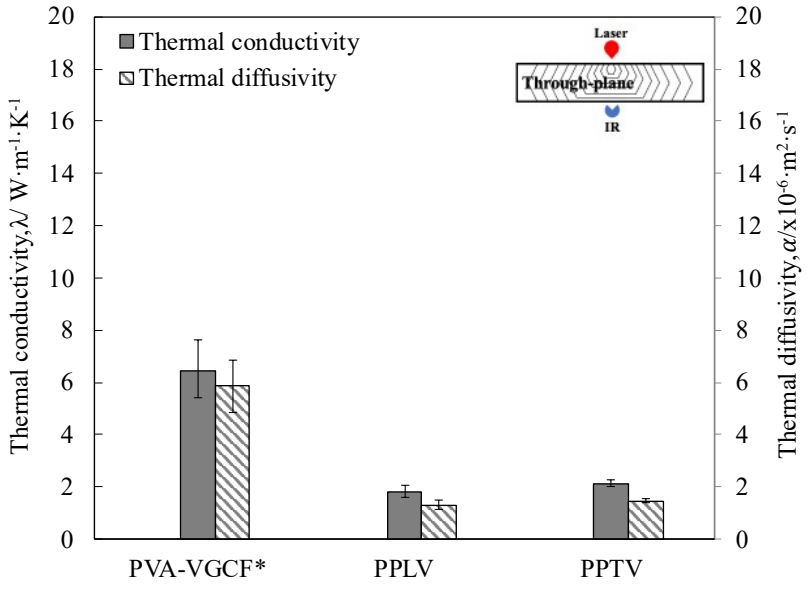

Fig. 3.7 Through-plane thermal conductivities and thermal diffusivities of PVA-VGCF, PPLV and PPTV sheet.

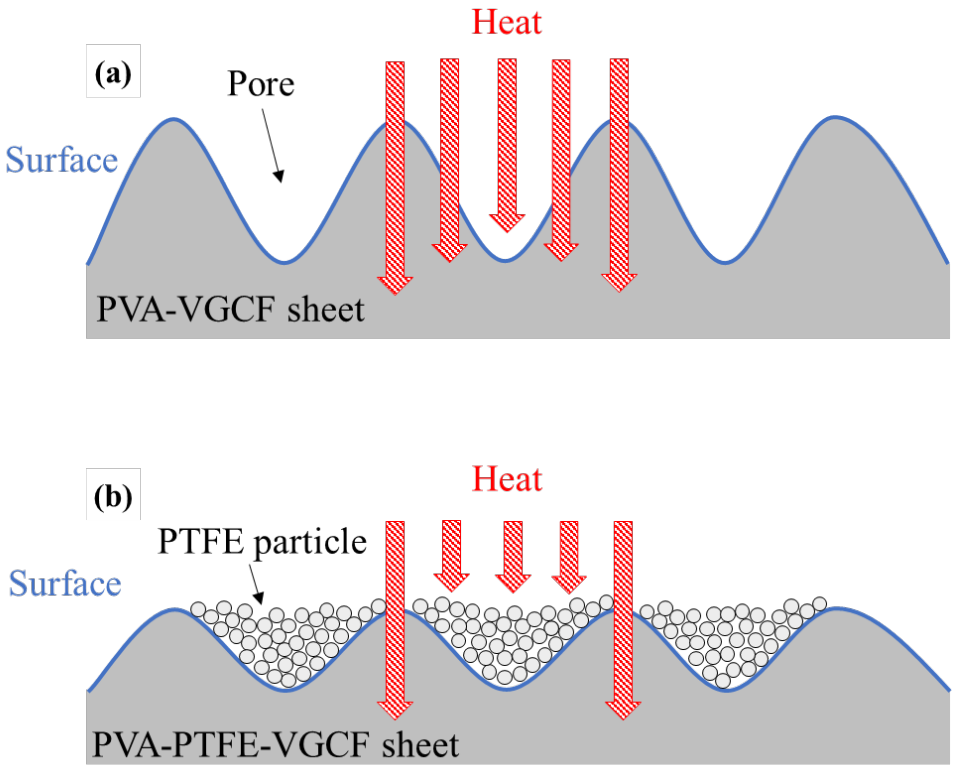

Fig. 3.8 The schematic of microstructure near the surface of PVA-VGCF sheet and PVA-PTFE-VGCF sheet.

Table 3.2 Comparison of thermal conductivity between this work and other paper-like composites.

Materials	Amount rate of reinforcement [wt.%]	Thermal conductivity [λ/W·m^{-1}·K^{-1}]		Ref.
		In-plane	Through-plane	
PPLV	27.78	7.66	1.79	This work
PPTV	27.78	9.81	2.11	This work
Graphene paper	Unknown	7.32	0.14	11
Cellulose/Ag composite film	2	6	0.8	12
Cellulose/Graphene Nanosheets Hybrid Films	1	12.6	0.042	13
Boron nitride nanosheet/cellulose nanofiber film	25	22.67	1.08	14
Graphene oxide /cellulose nanofiber composite films	50	7.3	0.13	15

3.3.4 High temperature and humidity test results

To evaluate the long-term performance, the PPLV and PPTV sheets were cut into specimens with a size of 20 × 20 mm for high temperature and humidity test. Each sample was kept at 358K and 85% RH for 500 hours. After the high temperature and humidity test, the in-plane and through-plane TC of each specimen were also measured. In Fig. 3.9, the SEM images of PPLV and PPTV sheets before and after the high temperature and humidity test was showed. It was clear to seen that the PVA in surface was partially disappeared after the test. As shown in Fig. 3.10, prior to testing, the in-plane TC of the PVA-VGCF sheet, PPLV sheet, and PPTV sheet were 14.30, 7.66, and 9.81 $W \cdot m^{-1} \cdot k^{-1}$, respectively; After testing, the TC of PVA-VGCF sheet was significantly reduced by 31% to 9.85 $W \cdot m^{-1} \cdot k^{-1}$. However, the TC of PPLV and PPTV sheets were increased to 9.02 and 10.81 $W \cdot m^{-1} \cdot k^{-1}$, with an increase of 18% and 10%. Similarly, as shown in and Fig 3.11, the through-plane TC of the PVA-VGCF sheet was decreased by 57% from 6.44 $W \cdot m^{-1} \cdot k^{-1}$ to 2.71 $W \cdot m^{-1} \cdot k^{-1}$ after the high temperature and humidity test. The TC of PPLV and PPTV sheets were increased from 1.79 and 2.11 W·m-1·k-1 to 2.21 and 2.49 $W \cdot m^{-1} \cdot k^{-1}$, with an increase of 23% and 18% respectively. In order to find out the reasons for the increased TC in PPLV and PPTV sheets, FT-IR analysis was performed on the surfaces of PPLV and PPTV sheets. The FT-IR result was shown in Fig. 3.12. Two IR detection bands were marked in this figure, 1211 cm^{-1} to 1154 cm^{-1} representing the entire C-F stretching of PTFE and a narrow band at 1734 cm^{-1} to 1717 cm^{-1} representing the C=O stretching of PVA. Before the high temperature and high humidity test, PVA and PTFE were detected on the surface of the fabricated VGCF sheet. However, after the high-temperature and humidity test, the C=O peak disappeared, which means that the PVA disappeared from the surface of the fabricated sheet. It is considered that due to the strong hydrophilicity of PVA, water molecules in the high-temperature and humidity test environment will be absorbed into the VGCF sheet by PVA. Water absorbed in PVA not only breaks hydrogen bonds but also provides more free volume and lubricity[16,17]. As a result, the PVA segments in the VGCF sheet

become easily mobile and respond quickly to load changes, which may cause the PVA to move from the surface to the central part of the VGCF sheet and lead to the disappearance of the C = O stretch in the FT-IR analysis. As a result, a large number of pores was generated on the surface of the VGCF sheet, resulting in a reduction of TC. Unlike PVA-VGCF sheets, the pores generated by PVA movement in PPLV and PPTV sheets can be effectively filled by PTFE particles. Therefore, due to the rearrangement of PVA and PTFE particles, PPLV and PPTV sheets obtained a uniform surface and higher density after high temperature and humidity tests. A TIM with a uniform surface tends to have a lower absolute thermal resistance, while a higher density helps increase the TC of the TIM. Therefore, the TC of PPLV and PPTV after high temperature and humidity test were increased. This phenomenon provides innovative ideas for improving the stability and long-term performance of TIMs in practical applications. The properties of each VGCF sheet were measured, and a comparison with referred PVA-VGCF sheet was shown in Fig. 3.13.

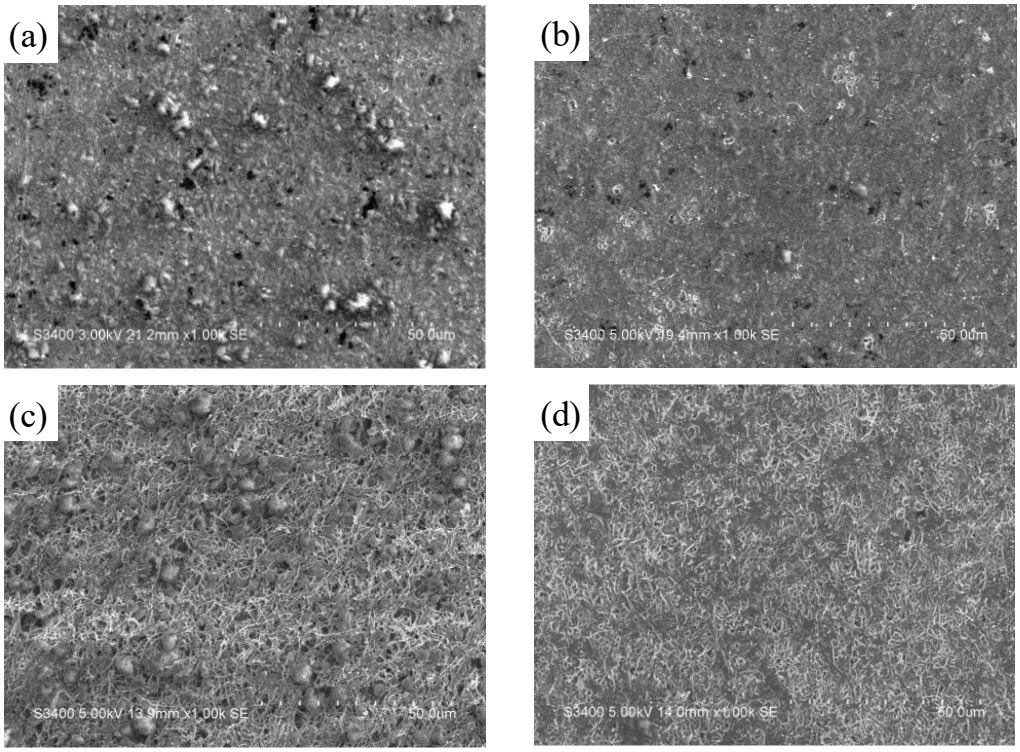

Fig. 3.9 SEM images(×1000) of (a)PPLV sheet, (b)PPTV sheet in room temperature and (c)PPLV sheet, (d)PPTV sheet after high temperature and humidity test.

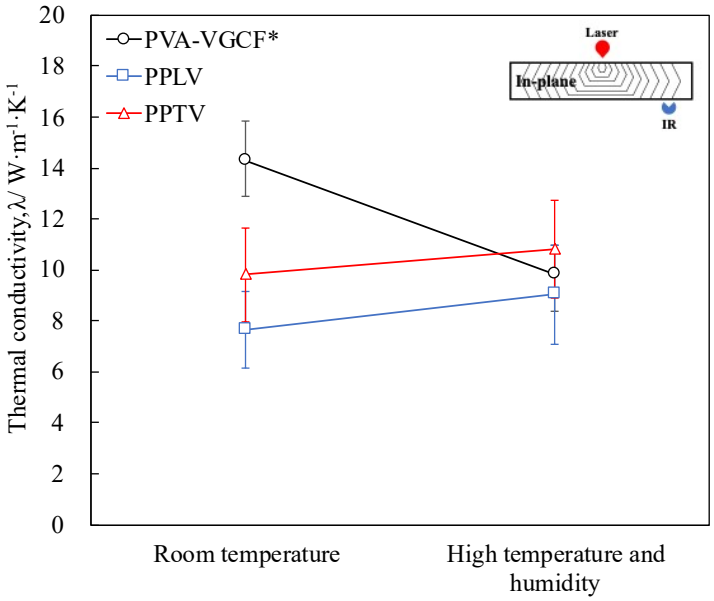

Fig. 3.10 The in-plane TC of fabricated CNF sheets after high temperature and humidity test.

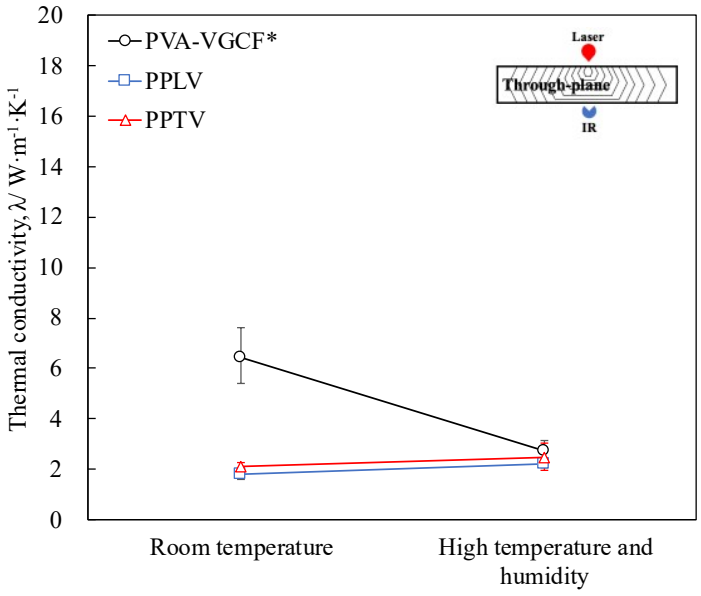

Fig. 3.11 The in-plane TC of fabricated CNF sheets after high temperature and humidity test.

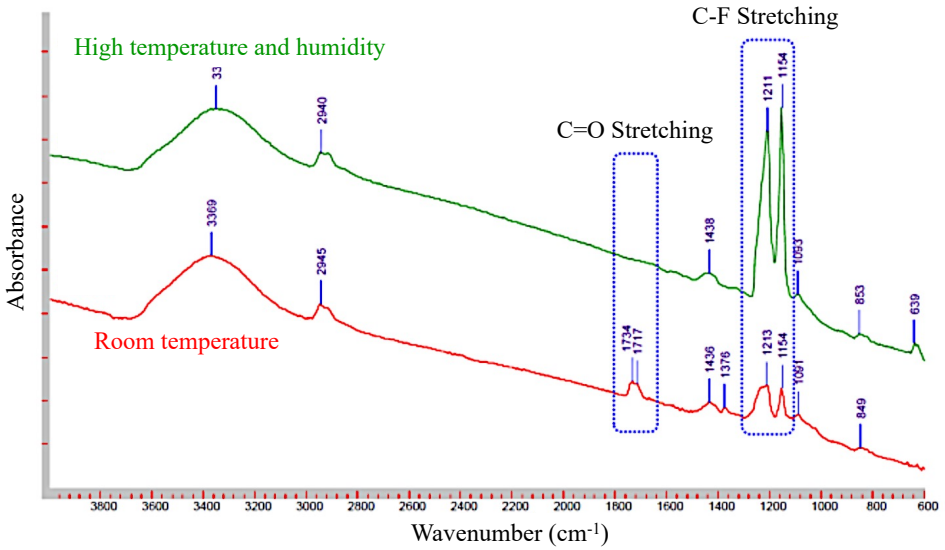

Fig. 3.12 The FT-IR analysis of fabricated CNF sheets at room temperature and after high temperature and humidity.

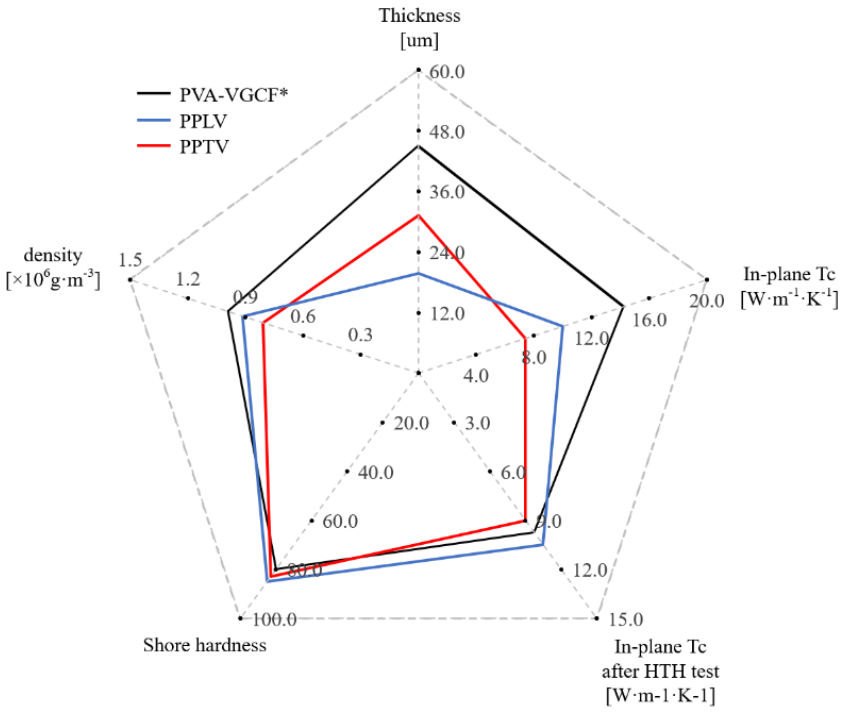

Fig. 3.13 The properties comparison of PVA-VGCF, PPLV and PPTV sheets.

3.4 Summary

A comparison with referred PVA-VGCF sheet was shown in Fig. 3.12. In all, novel PVA-PTFE-VGCF thermal interface materials were successfully developed by a simple and cost-effective process. Two types of VGCF sheets were fabricated by using 120nm and 300nm PTFE particles, the conclusions were summarized as follows:

(1) the microstructure observation revealed that the VGCFs were arranged in random directions and interconnected via PVA aggregates. 300nm PTFE particles were well distributed and compatible within the PPTV sheet, while partial aggregations of 120nm PTFE particles and unfilled pores were observed in the PPLV sheet.

(2) With the addition of PTFE particles, the thermal conductivities of fabricated CNF sheets were decreased. The fabricated PPTV sheet with PTFE size of 300nm has higher thermal conductivities of 9.81 $W \cdot m^{-1} \cdot k^{-1}$ in the in-plane direction and 2.11 $W \cdot m^{-1} \cdot k^{-1}$ in the through-plane direction.

(3) After the high temperature and humidity test, the in-plane and through-plane TC of PVA-PTFE-VGCF sheets were increased. According to the FT-IR analysis result, it was considered that the increase in TC was caused by the hydrophobic property of PVA and rearrangement of PVA and PTFE particles.

References

[1] Encyclopædia Britannica, Inc., USA, Available at. https://www.britannica.com/place/Antarctica/Plant-life (Accessed 2022-11-26).

[2] World Wide Fund For Nature, Switzerland, Available at. https://wwf.panda.org/discover/knowledge_hub/where_we_work/amazon/about_the_amazon/ (Accessed 2022-11-26).

[3] J. H. Ki, J. O. Hyun, E. Hyeonjin, K. Yeonsang, H. J. Jae: Sci. Total Environ. **783** (2021) 147083.

[4] M. G. Shi, F. M. Miyazawa, S. G. Tobe, T. A. Stolarski: Mater. Trans. **46** (2005) 84-87.

[5] ASTM International. ASTM D2240-15 Standard test method for rubber property-durometer hardness (2015).

[6] R. Sindhu, P. Binod, A. Pandey: Industrial Biorefineries & White Biotechnology (Elsevier B.V. 2015) pp. 575-605.

[7] J. L. Xiong, S.R. Chen, Y. B. Choi, K. Matsugi: Sci. Rep. **11** (2021) 17183.

[8] F. Zhang, Y.Y. Feng, M.M. Qin, L. Gao, Z.Y. Li, F.L. Zhao, Z.X. Zhang, F. Lv, W. Feng: Adv. Funct. Mater. **29** (2019) 1901383.

[9] J. Gu, G. Liang, X. Zhao, B. Gan, H. Qiu, Y. Guo, X. Yang, Q. Zhang, D.Y. Wang: Compos. Sci. Technol. **139** (2017) 83-89.

[10] C. P. Feng, L.Y. Yang, J. Yang, L. Bai, R.Y. Bao, Z.Y. Liu, M.B. Yang, H.B. Lan, W. Yang: Compos. Commun. **22** (2022) 100528.

[11] D. Jeon, S.H. Choi, W. Byon: Int. J. Heat Mass Transfer **132** (2019) 944-951.

[12] Z. M. Shen, J. C. Feng: ACS Appl. Mater. Interfaces **10** (2018) 24193-24200.

[13] N. Song, D. J. Jiao, S. Q. Cui, X. S. Hou, P. Ding, L.Y. Shi: ACS Appl. Mater. Interfaces **9** (2017) 2924-2932.

[14] Z. R. Hu, S. Wang, G. K. Chen, Q. Zhang, K. Wu, J. Shi, L.Y. Liang, M. G. Lu: Compos. Sci. Technol. **168** (2018) 287-295.

[15] W. X. Yang, Z. D. Zhao, K. Wu, R. Huang, T. Y. Liu, H. Liang, F. Chen, Q. Fu: J.

Mater. Chem. C **5** (2017) 3748-3756.

[16] R. J. Fong, A. Robertson, P. E. Mallon, R. L. Thompson: Polymers **10** (2018) 1036.

[17] R.M. Hodge, T.J. Bastow, G.H. Edward, G.P. Simon, A.J. Hill: Macromolecules **29** (1996) 8137-8143.

Chapter 4

Thermal simulation of PVA-VGCF sheet

4.1 Introduction

In the past, researchers typically use equation calculations to predict the thermal properties of materials. As showed in Table. 4.1, there are many typical thermal conductivity models to predicting the thermal conductivity of composite TIMs. Except of cumbersome calculations, these typical models also have limitations in usage case. For example, Maxwell-Eucken model is only valid in low volume fraction of fillers in TIM. And Eshelby model requires the fillers has no interacts between each other. Recently, many researchers have used the thermal simulation to demonstrate the thermal properties of their developed materials to obtain a more direct and clear expression with a relatively simple method than certified only by equation calculations. For example, W. Dai et al. build an evaluation system of Heater-TIM-Heat sink to investigate and compare the cooling performance between their developed new graphene TIM and state-of-the-art TIMs in real case[1]. C. P. Feng et al. also used the system of Heater-TIM-Heat sink to certify the thermal performance of paper like TIM fabricated by single layer Al_2O_3 and graphene nanoplatelets[2]. Many studies using thermal simulation to provide good results in predicting the thermal properties of TIM. Unsuitable concepts or fabrication condition can be discarded quickly without big cost of materials. A lot of features and options of the simulation system also reduce the temporary and apparatuses efforts compared to practical experiments. However, in these thermal simulations, the microstructure of developed TIM was seldom to be considered, the model of TIM is created as an equivalent to a single-phase material with uniform internal structure. Especially for fiber reinforced composite materials due to its complicated and randomly arrangement of fibers, studies are seldom focused on its thermal simulation based on the microstructures.

In this chapter, we prepared 5 types of three-dimensional model to present different arrangement of VGCFs in the fabricated CNF sheets through the CAE software ANSYS student. The goal of this chapter was to investigate the effect of VGCF arrangement on

the heat transfer in the fabricated sheets and develop a method using simulation data to predict the thermal conductivity of TIM.

Table 4.1 Typical thermal conductivity models for composite TIMs.

Model	Formula	Characteristics	Reference
Maxwell and Maxwell-Eucken	$\lambda_c = \lambda_m \frac{2 + \frac{\lambda_d}{\lambda_m} - 2V_m\left(1 - \frac{\lambda_d}{\lambda_m}\right)}{2 + \frac{\lambda_d}{\lambda_m} + V_m\left(1 - \frac{\lambda_d}{\lambda_m}\right)}$ $\lambda_c = \lambda_m \left[\frac{\lambda_f + 2\lambda_m - 2V_f(\lambda_m - \lambda_f)}{\lambda_f + 2\lambda_m + V_f(\lambda_f - \lambda_m)}\right]$	Used for continuous and uniformly distribution particles fillers in TIM. Inclusions of reinforcements isolated and dispersed in a continuously homogeneous matrix; it is only valid in low volume fraction of fillers	3-5
Bruggeman	$1 - V_f = \frac{\lambda_f - \lambda_c}{\lambda_f - \lambda_p}(\frac{\lambda_p}{\lambda_c})^{\frac{1}{3}}$	Dilute suspension of spheres in a homogeneous medium; It can be applied for high volume fraction of fillers.	6
Hasselman and Johnson	$K_{eff} = K_m \frac{2\left(\frac{K_f}{K_m} - \frac{K_f}{ah_c} - 1\right)V_f + \frac{K_f}{K_m} + \frac{2K_f}{ah_c} + 2}{\left(1 - \frac{K_f}{K_m} + \frac{K_f}{ah_c}\right)V_f + \frac{K_f}{K_m} + \frac{2K_f}{ah_c} + 2}$	This model is based on Maxwell model, and it considers the interfacial thermal resistance and the fillers size.	7
Eshelby	$K_{eff} = K_0 + c_1(K_1 - K_0)T$	Applied for Inhomogeneous spheres and the fillers don't interact with each other; Only valid in low volume of fillers	8
Tavangar	$K_c = K_m \frac{\frac{K_d^{eff}}{K_m}(1 + 2V_d) + (2 - 2V_d)}{\frac{K_d^{eff}}{K_m}(1 - V_d) + (2 + V_d)}$	This model is used for more than two components in TIM and can be applied for high volume fraction of fillers.	9
Mori Tanaka	$K_{eff} = \frac{c_0 K_0 + c_1 K_1 T}{c_0 I + c_1 T}$	This model considers the interactions of fillers and can be used for up to 20Vol% of fillers.	10,11
Ce-Wen Nan	$K_{eff} = K_m \frac{3 + 2f[\beta_x(1 - L_x) + \beta_z(1 - L_z)]}{3 - f(2\beta_x L_x + \beta_z L_z)}$	Applied for cylindrical dispersed dispersions in a 3D randomly oriented occasion. The model considers the anisotropy in thermal conductivity, the aspect ratio and volume fraction of the fillers as well as the interfacial thermal resistance.	12,13

4.2 Theory of thermal simulation

The main governing equation of the thermal simulation in this chapter is heat diffusion equation for conductive heat transfer. Solving this equation can achieves the main goal of conduction analysis, which is to predict the temperature distribution and heat flux in the TIM. In ANSYS system, the diffusion equation follows from the conservation of energy presented in three conditions: neglecting advection, assuming no mechanical work by surroundings and using internal energy in terms of enthalpy[14]. The diffusion equation can be described as:

$$\frac{\partial(\rho h)}{\partial t} = \nabla \cdot (k \nabla T) + S_g \tag{4.1}$$

This equation can be simplified by assuming constant density and specific heat capacity:

$$\rho c_p \frac{\partial T}{\partial t} = \nabla \cdot (k \nabla T) + S_g \tag{4.2}$$

where ρ is the density, c_p is the specific heat capacity, T is the temperature, t is time, k is the thermal conductivity and S_g is the heat generation source or heat sink. The physical meanings of heat diffusion equation are the rate of energy transfer into a unit volume by heat conduction, and plus the volumetric rate of heat generation is equal to the rate of change of heat stored within the volume. Then, the Cartesian form of the heat equation (4.2) can be described as[14]:

$$\rho c_p \frac{\partial T}{\partial t} = \frac{\partial}{\partial x}\left(k \frac{\partial T}{\partial x}\right) + \frac{\partial}{\partial y}\left(k \frac{\partial T}{\partial y}\right) + \frac{\partial}{\partial z}\left(k \frac{\partial T}{\partial z}\right) + S_g \tag{4.3}$$

In this form of heat equation, $\rho c_p \frac{\partial T}{\partial t}$ represents the rate of change of heat stored, $\frac{\partial}{\partial \mathrm{x}}\left(k \frac{\partial T}{\partial x}\right) + \frac{\partial}{\partial \mathrm{y}}\left(k \frac{\partial T}{\partial y}\right) + \frac{\partial}{\partial \mathrm{z}}\left(k \frac{\partial T}{\partial z}\right)$ represents the rate of transfer by conduction and S_g is the rate of heat generation source. Furthermore, in the case of constant thermal conductivity, equation (4.3) can be reduced to[15]:

$$\frac{1}{\alpha}\frac{\partial T}{\partial t} = \frac{\partial^2 T}{\partial x^2} + \frac{\partial^2 T}{\partial y^2} + \frac{\partial^2 T}{\partial z^2} + \frac{S_g}{k} \tag{4.4}$$

where the property $\alpha = k/\rho c$ is the thermal diffusivity of the material. Equation (4.4) is also known as Fourier-Biot equation. Besides, this equation reduces to these forms

under specific conditions, Poisson equation for steady-state condition:

$$\frac{\partial^2 T}{\partial x^2}+\frac{\partial^2 T}{\partial y^2}+\frac{\partial^2 T}{\partial z^2}+\frac{S_g}{k}=0 \tag{4.5}$$

Diffusion equation for transient and no heat generation condition:

$$\frac{1}{\alpha}\frac{\partial T}{\partial t}=\frac{\partial^2 T}{\partial x^2}+\frac{\partial^2 T}{\partial y^2}+\frac{\partial^2 T}{\partial z^2} \tag{4.6}$$

Laplace equation for steady-state and no heat generation condition:

$$\frac{\partial^2 T}{\partial x^2}+\frac{\partial^2 T}{\partial y^2}+\frac{\partial^2 T}{\partial z^2}=0 \tag{4.7}$$

practical case of planar conduction as showed in Fig. 4.1, the heat conduction equation is:

$$T(x)=T_1-(T_1-T_1)\frac{x}{L} \tag{4.8}$$

The heat transfer rate q_x and heat flux q_x'' can be derived from Fourier's Law:

$$q_x=-kA\frac{dT}{dx}=\frac{kA}{L}(T_1-T_1) \tag{4.9}$$

$$q_x''=\frac{q_x}{A}=\frac{k}{L}(T_1-T_1) \tag{4.10}$$

where A is wall area normal to the heat transfer direction. And thermal resistance of planar conduction is:

$$R_t=\frac{L}{kA} \tag{4.11}$$

Furthermore, for the heat conduction in multiple layers of composite walls as shown as Fig. 4.2, thermal resistance is additive by a linear increase. The heat transfer through multiple layers can be derived from the sum of thermal resistance:

$$R_{total}=\sum R_{ti} \tag{4.12}$$

$$q_x=\frac{T_1-T_4}{R_{total}} \tag{4.13}$$

It should be noted that in this chapter, the steady-state condition was chosen for thermal simulation, therefore the heat transfer under transient and unsteady condition was not discussed.

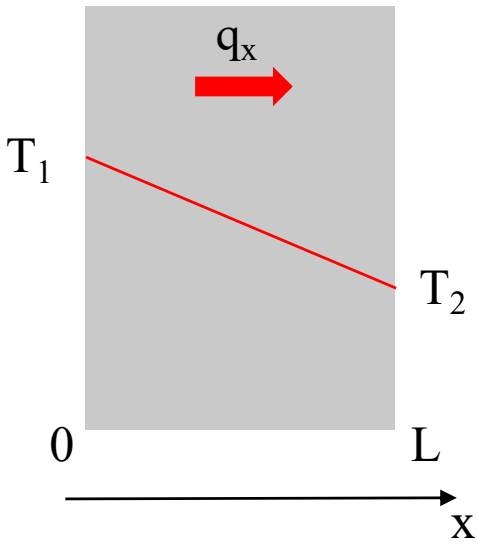

Fig. 4.1 Schematic of 1D planar conduction.

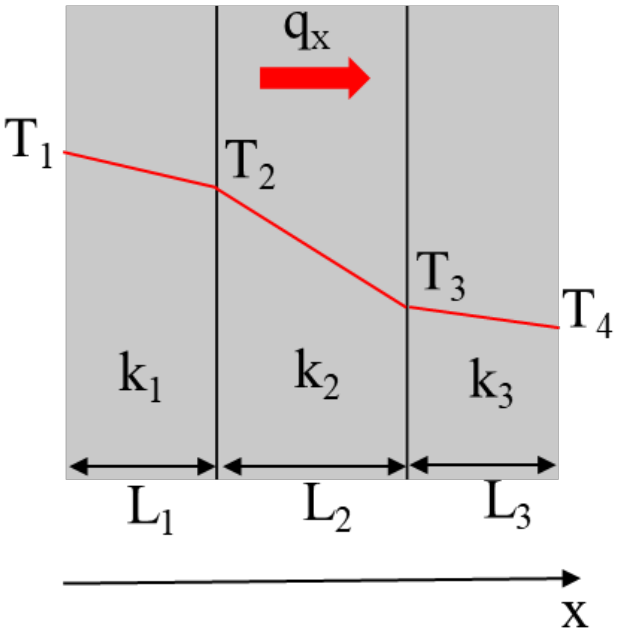

Fig. 4.2 Schematic of heat conduction through multiple layers.

4.3 Methodology of thermal simulation

4.3.1 Workflow

As showed in Fig. 4.3, a simplified workflow for thermal simulation in this chapter was introduced. There were totally 7 steps need to finish during the thermal simulations. In table 4.2, terms of thermal simulation and its units was listed. Table 4.3 showed the major physical parameters used in this thermal simulation. The λ_1, λ_2, λ_3, ρ_1, ρ_2, ρ_3 and c_{p1}, c_{p2}, c_{p3} represent the thermal conductivity, density and specific heat capacity of PVA, VGCF and Copper, respectively. The T_H, T_C represent the set temperature of heater, cooler, respectively. The T_{In} is ambient set temperature.

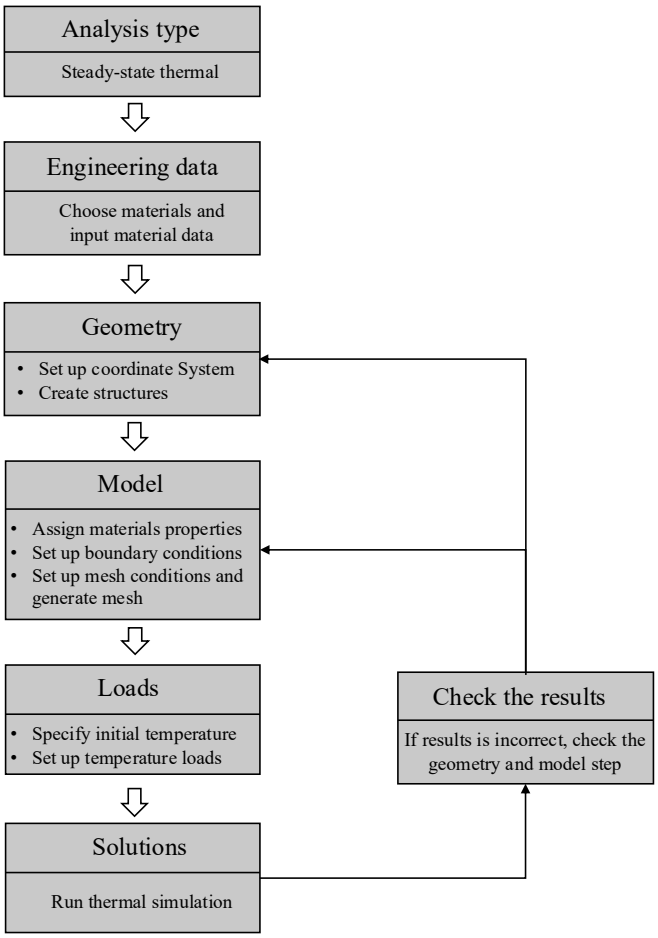

Fig. 4.3 A workflow for thermal simulation in this chapter.

Table 4.2 Terms of thermal analogy used in the simulation.

Thermal analysis item, [units], symbol
Temperature [K], T
Temperature gradient [K·m^{-1}], ∇T
Heat Flux [W·m^{-2}], q
Heat source for point, line, surface, volume [W], [W·m^{-1}], [W·m^{-2}], [W·m^{-3}], Q
Thermal conductivity [W·m^{-1}·K^{-1}], λ
Specific heat capacity [J·kg^{-1}·K^{-1}], c_p
Density [kg·m^{-3}], ρ

Table 4.3 Major physical parameters used in the simulation.

Major physical parameters		
λ_1=0.5 W·m^{-1}·K^{-1}	λ_2=1200 W·m^{-1}·K^{-1}	λ_3=386 W·m^{-1}·K^{-1}
ρ_1=1250 kg·m^{-3}	ρ_2=2100 kg·m^{-3}	ρ_3=8960 kg·m^{-3}
c_{p1}=2.5 J·kg^{-1}·K^{-1}	c_{p2}=700 J·kg^{-1}·K^{-1}	c_{p3}=384 J·kg^{-1}·K^{-1}
T_H=373K	T_C=293K	T_{In}=293K

4.3.2 Geometry

In the geometry step of thermal simulation, the PVA-VGCF sheet was chosen as simulate object firstly and the porosity was not considered. As showed in Fig. 4.4, we divided the CNF sheet into many small basic units and created geometry of basic unit. The size of a small basic unit was set up as 15um×15um×15um to keep the aspect ratio of VGCF(diameter:0.15um,average length:15um, aspect ratio:100). The reason for using basic unit instead of the whole CNF sheet was it is impossible to create a TIM model directly with countless VGCFs in it. Too many objects in the geometry can significantly increase the difficulty of the solution step. If it is necessary in the future research, TIM can be formed by stacking these basic units together. The size of TIM also can be controlled through adding or reducing the number of basic units. In Fig. 4.5 To evaluate the effect of the arrangements of VGCFs on the thermal conduction of fabricated PVA-VGCF sheet, 5 types of microstructure models were designed: pure PVA, horizontally arranged VGCF in PVA matrix, vertically arranged VGCF in PVA matrix, randomly arranged VGCF in PVA matrix and pure VGCF. For the cases where VGCF was added, the number of added VGCF was 100 and the volume fraction ratio of VGCF was about 3.13 vol%. Especially for the models of horizontally arranged VGCF in PVA, vertically arranged VGCF in PVA, the VGCFs was set up as a diameter of 0.15um, length of 15um and 1.67um apart from each other. Furthermore, as shown as Fig. 4.6, those 5 models were inserted respectively between a heater and cooler with same size of 15um×15um×15um in geometry step. The Heater-material-Cooler system was created to investigate the heat transfer path and thermal conductivity for 5 models consisting of PVA and VGCF. The cooper was set up as the material of heater and cooler.

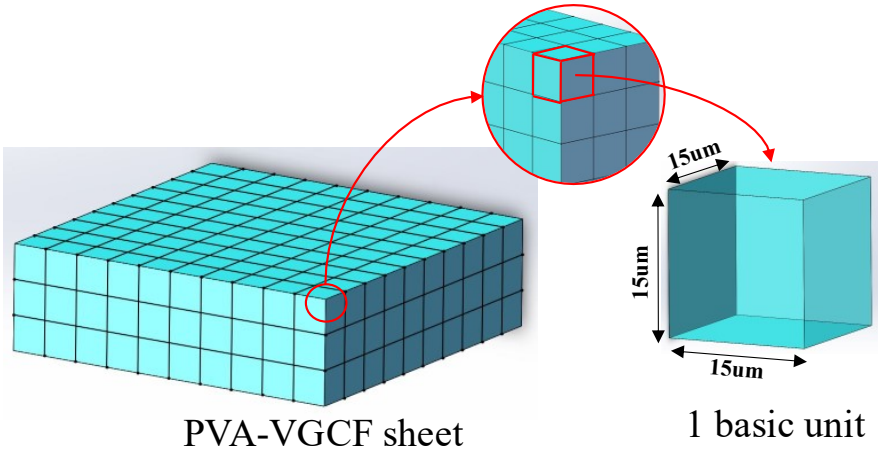

Fig. 4.4 The schematic of the basic unit of fabricated CNF sheet.

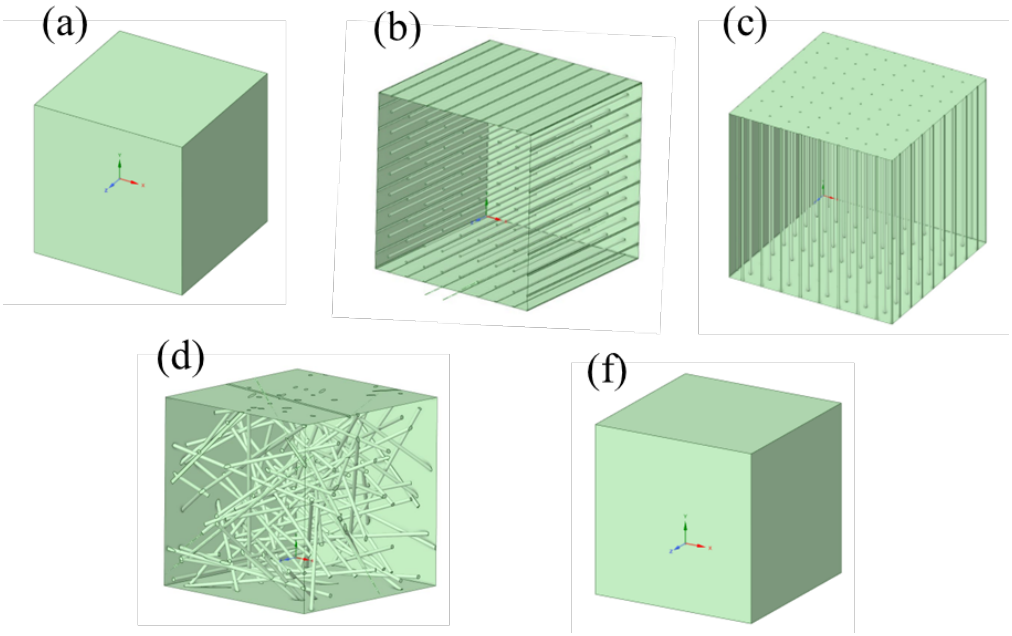

Fig. 4.5 Five types of geometry model: (a) pure PVA; (b) horizontally arranged VGCF in PVA matrix; (c) vertically arranged VGCF in PVA matrix; (d) randomly arranged VGCF in PVA matrix; (f) pure VGCF.

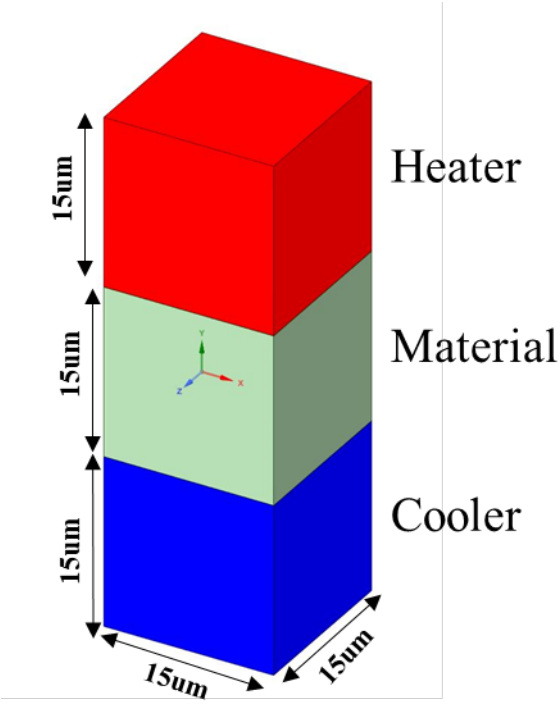

Fig. 4.6 Geometry model of Heater-Material-Cooler system in this thermal simulation.

4.3.3 Model

In this thermal simulation, the boundary condition was set up as bonded without considering the existence of pores in models, which means the PVA and VGCF were tightly bonded together in the contact surface. Other boundary conditions such as formulation and thermal conductance, were set up to controlled by the software program.

During the mesh step, the mesh size was used to control the mesh equality of models. Mesh size determine the size of elements, it is one of the most common problems in simulation. Too big elements give bad results, but too small elements make computing so long and give the risk of failing in solution step. Usually, reducing the element size in places where the main thermal conduction existed is an efficient way for set up mesh size. Therefore, in this simulation, since the heater and cooler were not very critical parts in the heat transfer process and reducing the number of elements can reduce the time and difficulty of the solution step, the mesh size of the heater and cooler was set to 1.5um. The mesh size of PVA was decreased to 0.5um and mesh size of VGCF was refined to 0.15um to increase accuracy of heat conduction results. The image and statistics of mesh results is showed in Fig. 4.7.

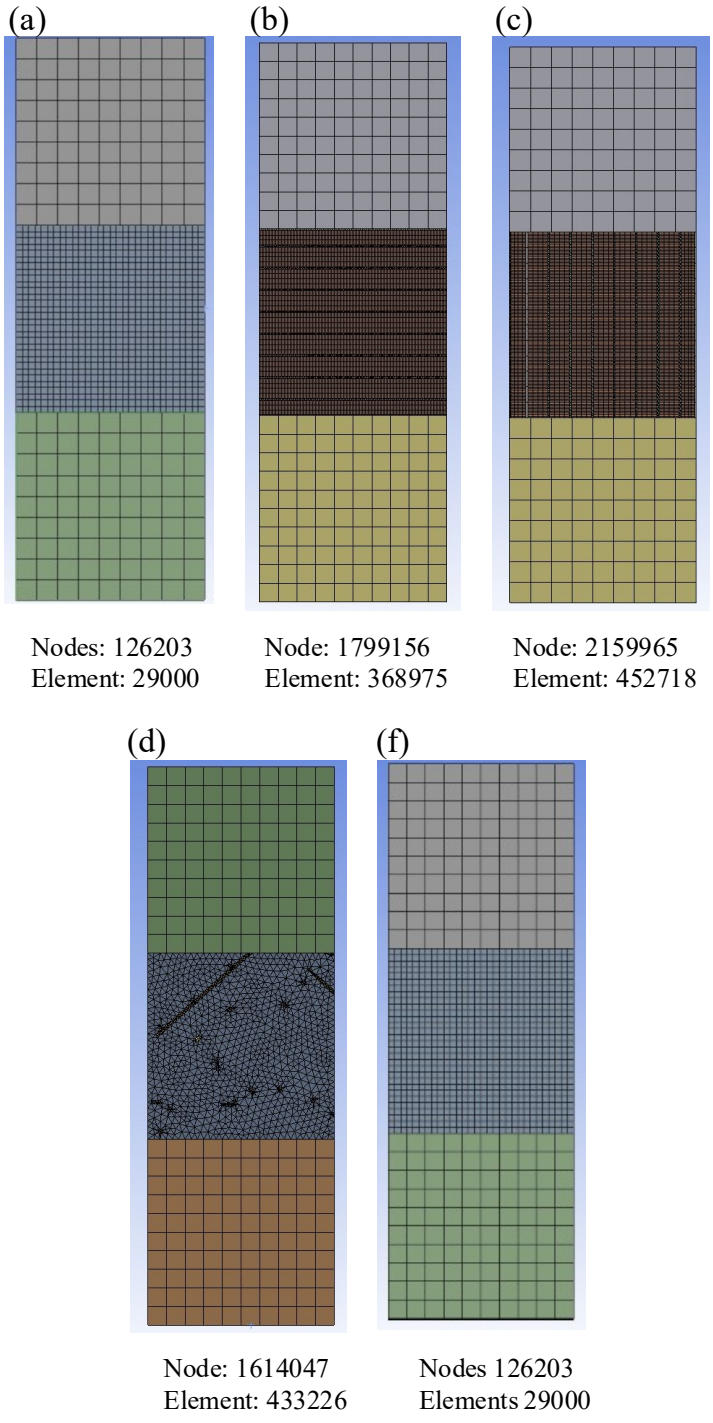

Fig. 4.7 The images and statistics of mesh results of model: (a) pure PVA; (b) horizontally arranged VGCF in PVA matrix; (c) vertically arranged VGCF in PVA matrix; (d) randomly arranged VGCF in PVA matrix; (f) pure VGCF.

4.3.4 Solution setup

In this simulation, the solution setup includes loads setup and analysis results setup. As showed in Fig. 4.8, the top face of heater was set up to 373K and bottom face of cooler was set up to 293K in loads setup. The initial temperature and the ambient temperature were assumed to be equal as 293K. The fixed time stepping method was used in the simulation. The time step size and number of time steps were 1 s and 1000, respectively. The analysis results were set to temperature distribution and heat flux distribution.

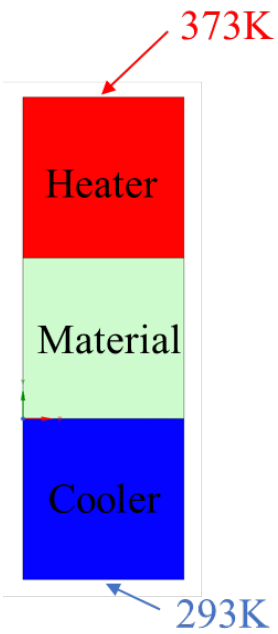

Fig. 4.8 Image of temperature setup for simulation.

4.4 Results

4.4.1 Temperature distribution

Fig. 4.9 shows the images of temperature distribution results of 5 models. The models of pure PVA, horizontally arranged VGCF in PVA and vertically arranged VGCF in PVA showed a similar distribution of temperature. The temperature decreased from heater to cooler, while the change of temperature was mainly concentrated on the region of the test material which dropped from 363K to 303K. As for the material of randomly arranged VGCF in PVA, the temperature also had a significant drop in the test material region and the temperature distribution had obvious fluctuations along the VGCF direction which was showed in Fig. 4.9(d). To material of pure VGCF, the temperature distribution exhibited a uniform distribution from top of heater to bottom of cooler, and the temperature of test materials region only dropped from 338K to 325K. The better the thermal conductivity of the TIM is, the easier for TIM to help the heat source transfer heat to the heat sink and forms a more uniform temperature distribution of whole system.

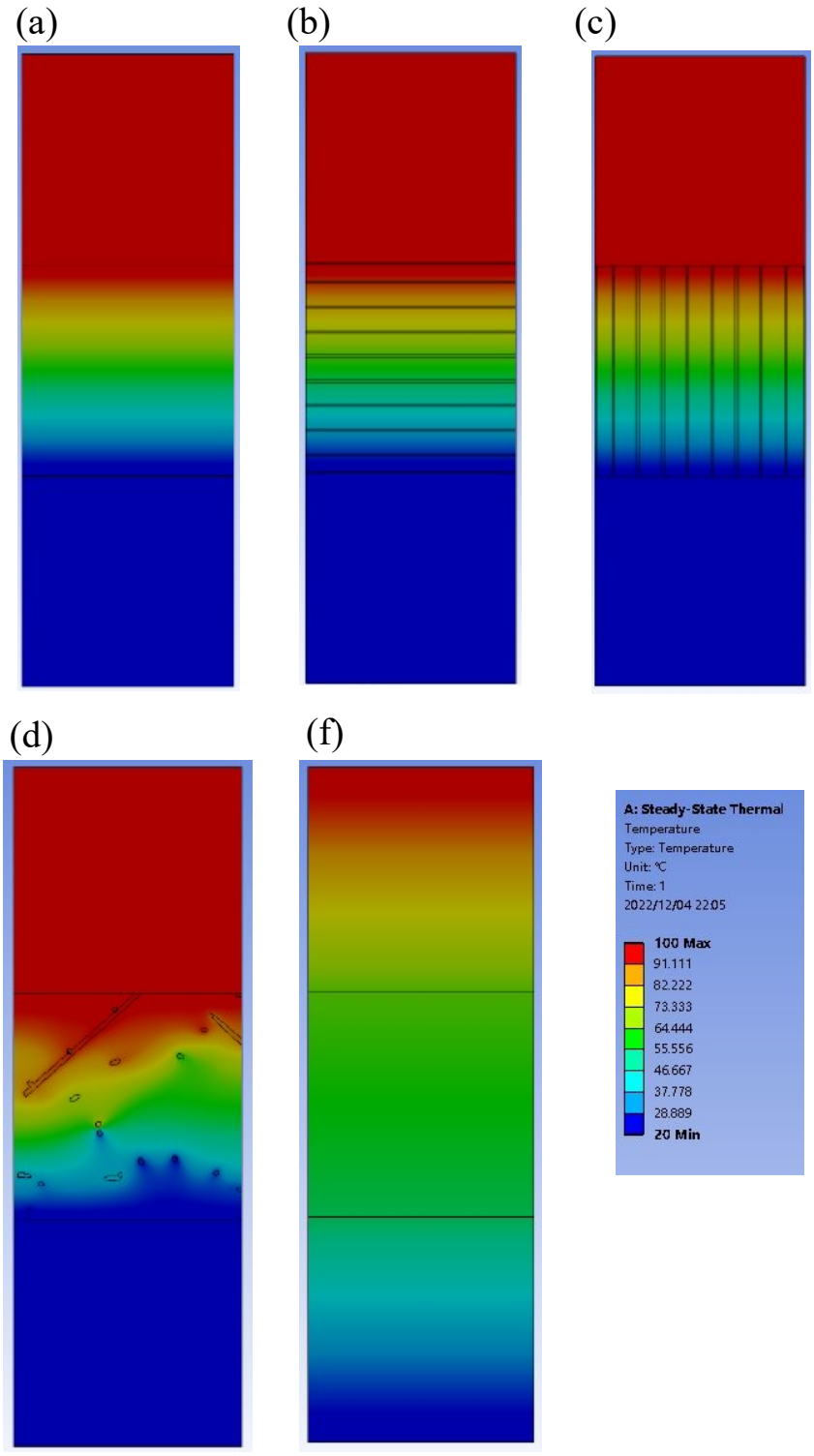

Fig. 4.9 Images of temperature distribution results of the model: (a) pure PVA; (b) horizontally arranged VGCF in PVA matrix; (c) vertically arranged VGCF in PVA matrix; (d) randomly arranged VGCF in PVA matrix; (f) pure VGCF.

4.4.2 Heat flux distribution

Fig. 4.10 shows the images of heat flux distribution of 5 models and Table 4.4 gives the statistics of heat flux of them. Pure PVA and pure VGCF models had the constant heat flux distribution value respectively due to their single-phase microstructure. But because of the huge difference of thermal conductivity(PVA:0.5 $W \cdot m^{-1} \cdot K^{-1}$, VGCF: 1200 $W \cdot m^{-1} \cdot K^{-1}$), the average heat flux in pure PVA model was just 2.66 $W \cdot m^{-2}$, while that in pure VGCF model was as high as 886.64 $W \cdot m^{-2}$, which also demonstrated that heat transfer was very slow in pure PVA model and need much time to reach the steady-state condition. As for the left 3 models: horizontally arranged VGCF, vertically arranged VGCF and randomly arranged VGCF in PVA matrix, Fig. 4.11 provide more details about heat flux distribution and vectors pictures which shows the transfer direction of heat. Due to lacking efficient heat transfer path, the model of horizontally arranged VGCF showed very low heat flux data, which was almost similar to pure PVA. As for the model of vertically arranged VGCF, each single vertical VGCF connected heater and cooler, which provided many efficient heat transfer paths for the materials. Thus, there were high value of heat flux results. Neither like model of horizontally arranged VGCF which completely lacked effective heat transfer paths, nor similar to model of vertically arranged VGCF which had many paths, from the Fig. 4.12 it was showed that the efficient heat transfer paths in model of randomly arranged VGCF were created only by the interleaved VGCFs and connected to each other. Also, the direction of heat transfer was severely affected by the VGCF alignment direction as showed in Fig. 4.11(c). Thus, increasing the amount of thermally conductive fillers would contribute to an increasement of thermal conductivity by increasing the number of intersections between fillers. Overall, heat transfer in TIM with randomly arranged fillers mainly depends on the efficient heat transfer path created by interactions of thermally conductive fillers. Without efficient heat transfer paths, the heat transfer would not follow the direction from the heat source to the heat sink as we hoped but

may towards other directions disorderly, or even almost stop.

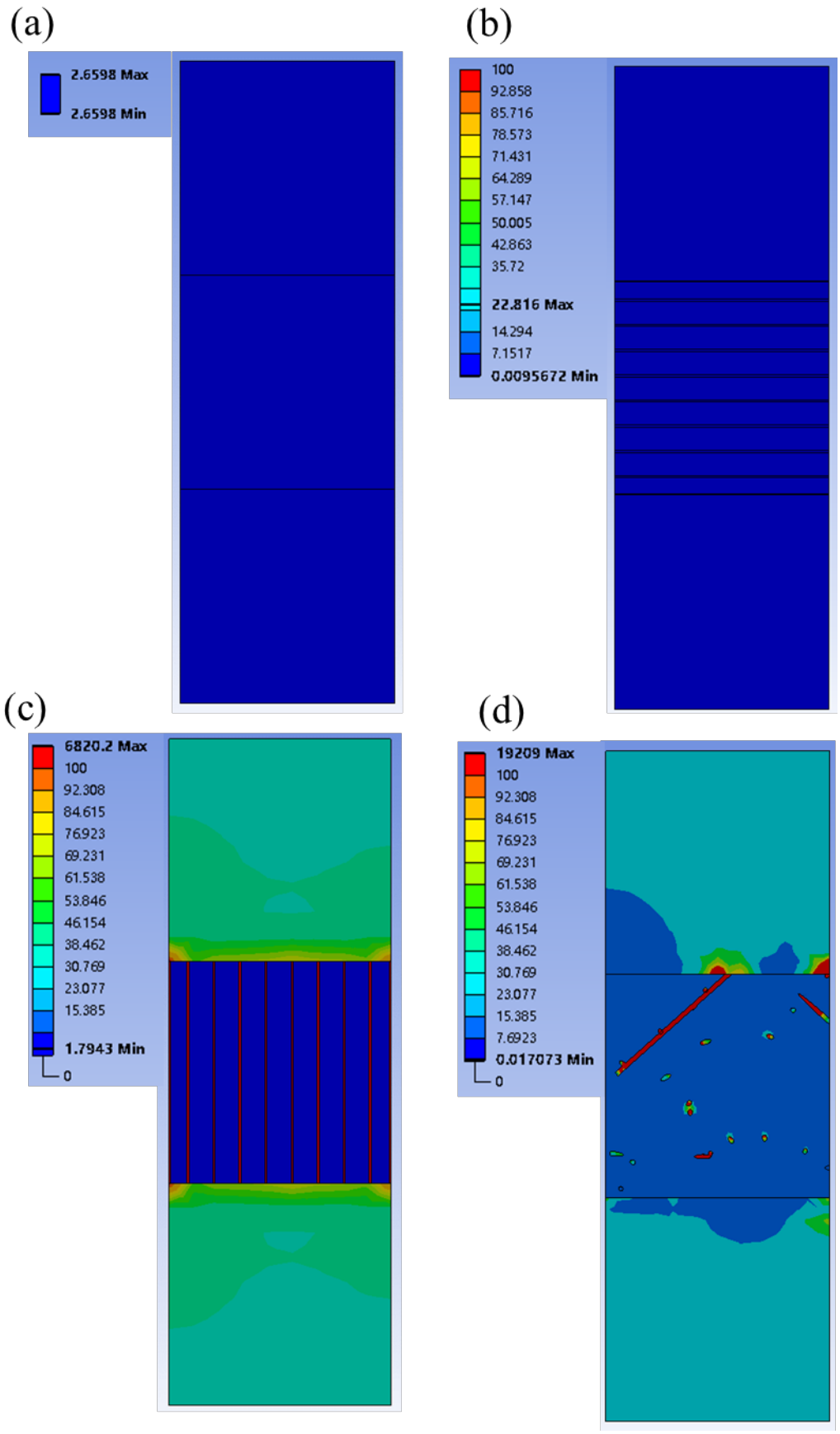
(a)
2.6598 Max
2.6598 Min
(b)
100
92.858
85.716
78.573
71.431
64.289
57.147
50.005
42.863
35.72
22.816 Max
14.294
7.1517
0.0095672 Min
(c)
6820.2 Max
100
92.308
84.615
76.923
69.231
61.538
53.846
46.154
38.462
30.769
23.077
15.385
1.7943 Min
0
(d)
19209 Max
100
92.308
84.615
76.923
69.231
61.538
53.846
46.154
38.462
30.769
23.077
15.385
7.6923
0.017073 Min
0

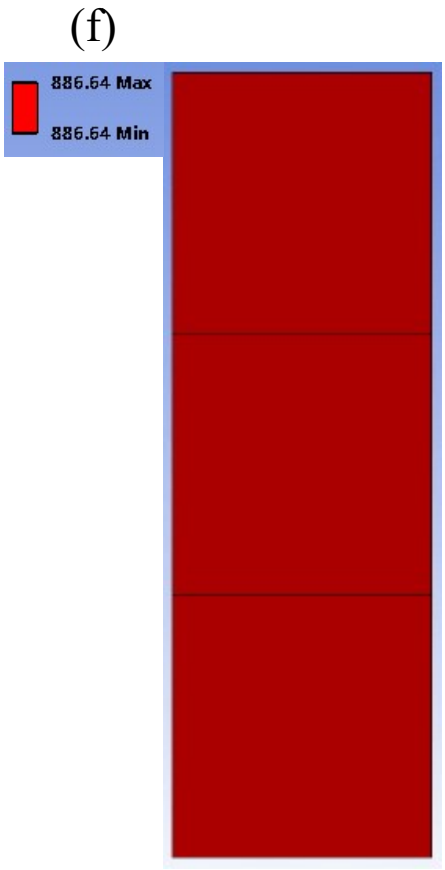

Fig. 4.10 Images of heat flux distribution results of model: (a) pure PVA; (b) horizontal arranged VGCF in PVA matrix; (c) vertical arranged VGCF in PVA matrix; (d) randomly arranged VGCF in PVA matrix and (f) pure VGCF.

Table 4.4 Statistics of total heat flux of each model.

Model	Heat flux [q/W·m^{-2}]		
	Minimum	Maximum	Average
Pure PVA	2.6598	2.6598	2.6598
horizontally arranged VGCF+PVA	0.0095	22.8	3.5
Vertically arranged VGCF+PVA	1.7943	6820.2	2780.8
randomly arranged VGCF+PVA	0.0171	19209.0	624.3
Pure VGCF	886.64	886.64	886.64

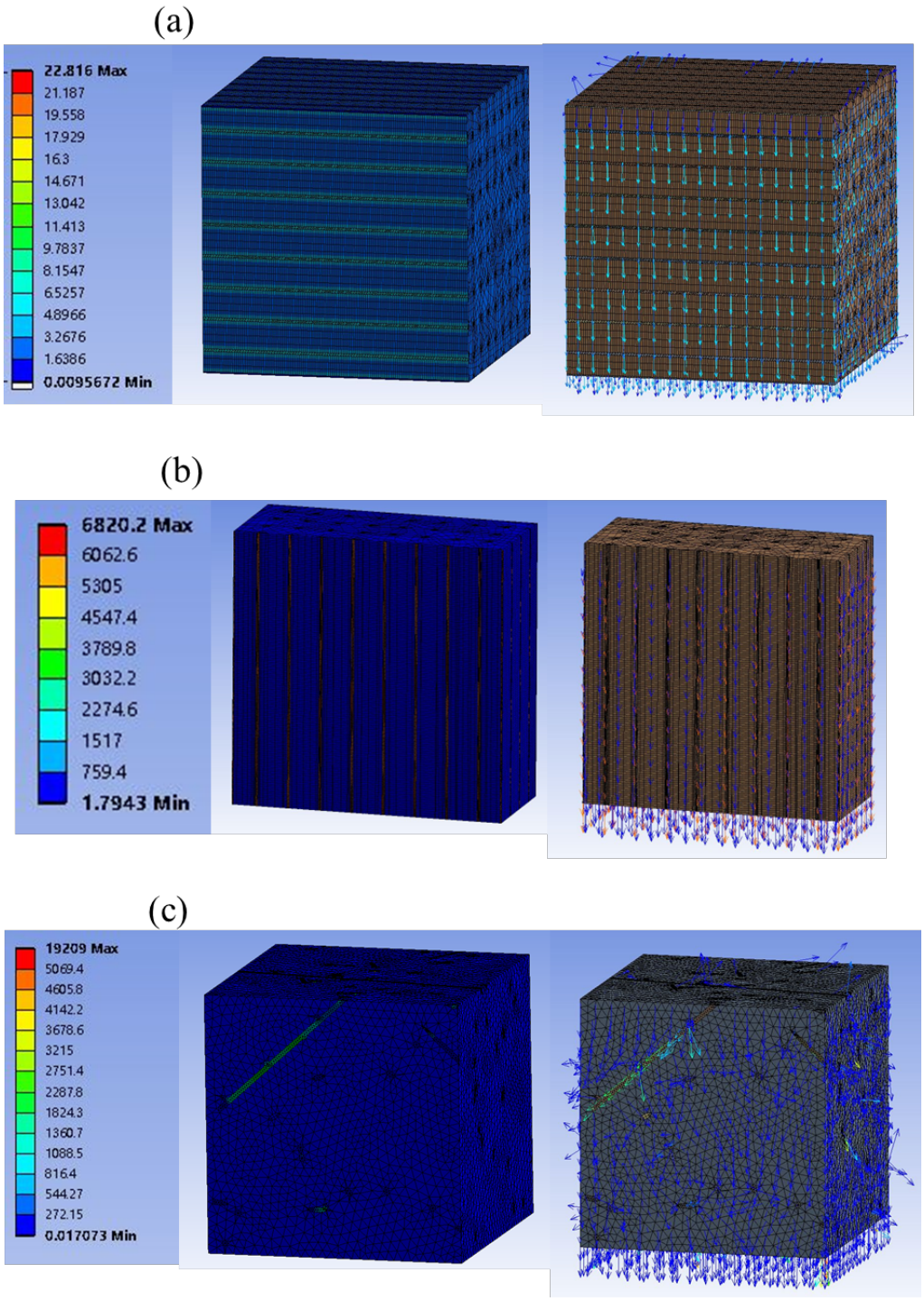

Fig. 4.11 Detail images of heat flux distribution results of: (a) horizontally arranged VGCF in PVA matrix; (b) vertically arranged VGCF in PVA matrix; (c) randomly arranged VGCF in PVA matrix.

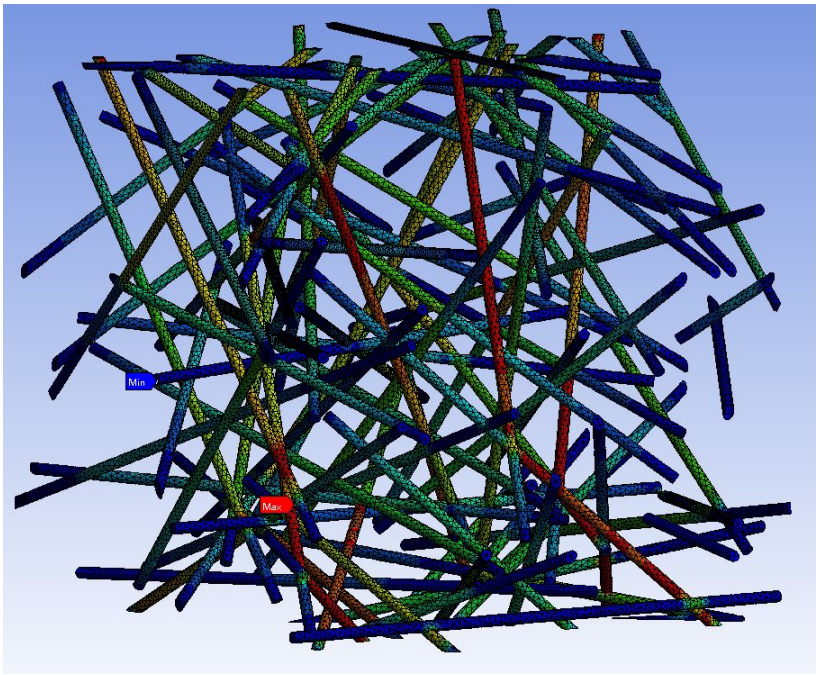

Fig. 4. 12 Image of heat flux distribution results of only VGCF in the model of randomly arranged VGCF.

4.4.3 Thermal conductivity

As showed in Fig. 4. 13, the steady-state method was used to calculate the thermal conductivity of 5 models. Assuming that the temperature gradients of heater, material and cooler are a_h, a_s, a_c, they are expressed by the following equations:

$$a_h = \sum_{i=1}^{3}(z_i - \overline{z}_h)(T_i - \overline{T}_h) / \sum_{i=1}^{3}(z_i - \overline{z}_h)^2,\ \overline{z}_h = \frac{1}{3}\sum_{i=1}^{3} z_i, \overline{T}_h = \frac{1}{3}\sum_{i=1}^{3} T_i \qquad (4.14)$$

$$a_s = \sum_{i=4}^{6}(z_i - \overline{z}_h)(T_i - \overline{T}_h) / \sum_{i=4}^{6}(z_i - \overline{z}_h)^2,\ \overline{z}_h = \frac{1}{3}\sum_{i=4}^{6} z_i, \overline{T}_h = \frac{1}{3}\sum_{i=4}^{6} T_i \qquad (4.15)$$

$$a_c = \sum_{i=7}^{9}(z_i - \overline{z}_h)(T_i - \overline{T}_h) / \sum_{i=7}^{9}(z_i - \overline{z}_h)^2,\ \overline{z}_h = \frac{1}{3}\sum_{i=7}^{9} z_i, \overline{T}_h = \frac{1}{3}\sum_{i=7}^{9} T_i \qquad (4.16)$$

where z_i and T_i are the distance and temperature of the number *i* thermal couple from heating plate. Effective thermal conductivity λ_x can be calculated by the following equation:

$$\lambda_x = \frac{\lambda_R(a_h + a_s)}{a_c} \qquad (4.17)$$

For the example showed Fig. 4.14, the temperature data of 9 point was taken from the surface of pure PVA model by a same distance of 4.5um. Through equation (4.14)~(4.17), the thermal conductivity of pure PVA model can be calculated as 0.497 $W \cdot m^{-1} \cdot K^{-1}$, which was almost the same as the reference value of 0.5 $W \cdot m^{-1} \cdot K^{-1}$. The thermal conductivity of 5 models was summarized in table 4.5. By compared the thermal conductivity of pure PVA and pure VGCF to the reference data(PVA:0.5 $W \cdot m^{-1} \cdot K^{-1}$, VGCF:1200 $W \cdot m^{-1} \cdot K^{-1}$), it was obvious that using thermal simulation results to predict the thermal conductivity of materials is feasible and the results is deserved to be trust. From the table, it can be seen that due to the lack of heat transfer path, microstructure model of horizontally arranged VGCF exhibited the almost the same low thermal conductivity(0.509 $W \cdot m^{-1} \cdot K^{-1}$) as pure PVA. For the model with vertically arranged

VGCF, its thermal conductivity was as high as 8.238 $W \cdot m^{-1} \cdot K^{-1}$, which had an ideal arrangement of conductive fillers for TIM. As mentioned in Chapter 1, this vertical arrangement of fillers requires complex manufacturing process and high cost, which is hard to achieve in practical application. As for the microstructure model of randomly arranged VGCF, although the thermal conductivity of it was relatively lower(4.600 $W \cdot m^{-1} \cdot K^{-1}$) than that of vertically arranged VGCF model, the thermal conductivity can be improved significantly by increasing the amount of VGCF. The increasement of VGCF would contribute to more VGCF interactions and provide additional heat transfer paths in the materials. In general, from the microstructure to the macroscopic performance, the number of efficient heat transfer paths was determined by the arrangement of the conductive fillers in TIM, meanwhile the thermal conductivity of the whole material was determined by the heat transfer paths in it.

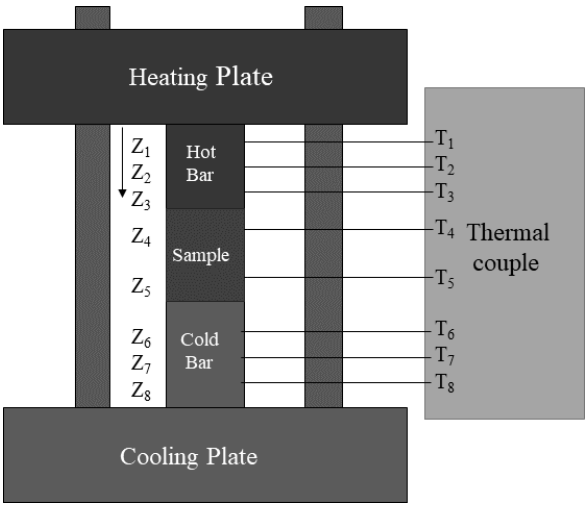

Fig. 4.13 Schematic of steady-state method for thermal conductivity measurement.

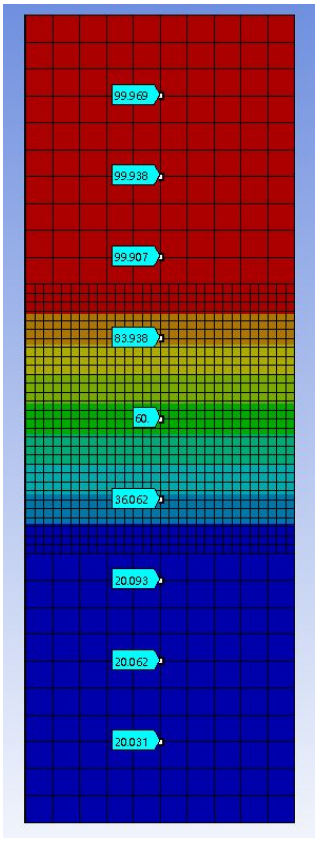

Fig. 4.14 Image of temperature data of 9 points used for thermal conductivity calculation in pure PVA model.

Table 4.5 The summarized thermal conductivity of fabricated models.

Model	Thermal conductivity [λ/W·m^{-1}·K^{-1}]
Pure PVA	0.497
Horizontally arranged VGCF+PVA	0.509
Vertically arranged VGCF+PVA	8.238
Randomly arranged VGCF+PVA	4.600
Pure VGCF	1193.749

4.5 Summary

In this chapter, 5 types of simulation models were created successfully: pure PVA, horizontally arranged VGCF in PVA matrix, vertically arranged VGCF in PVA matrix, randomly arranged VGCF in PVA matrix and pure VGCF. To investigate the heat transfer path and thermal conductivity of them, they were combined with a heater and a cooler to measure the thermal simulations, the main conclusions are as follows:

(1) Material models of pure PVA, horizontally arranged VGCF and vertically arranged VGCF in PVA showed a change of temperature mainly concentrated on the region of the test material. Temperature distribution of randomly arranged VGCF model had obvious fluctuations along the VGCF direction. The temperature distribution of pure VGCF model exhibited a uniform distribution from top of heater to bottom of cooler.

(2) Heat transfer was severely affected by the VGCF arrangement in material models. To the material model of randomly aligned VGCF in PVA, increasing the amount of VGCF would contribute to an increasement of thermal conductivity by increasing the number of intersections between VGCFs.

(3) An attempt on predicting thermal conductivity of material by using thermal simulation results was succeeded. Compared with the horizontally and randomly arrangement of VGCF, the vertically arrangement of VGCF has been shown to contribute significantly to the enhancement of thermal conductivity. If there were no efficient heat transfer paths, the thermal conductivity would be as low as PVA matrix.

References

[1] W. Dai et al.: ACS Nano **13** (2019) 11561-11571.

[2] C. P. Feng et al: Chem. Eng. J. **392** (2020) 123784.

[3] J. C. Maxwell: Pergamon, Oxford, vol. 1. 3rd ed. 1904.

[4] J. Z. Xu, B. Z. Gao, F. Y. Kang: Appl. Therm. Eng. **102** (2016) 972-979.

[5] A. Eucken: Forschung Gabiete Ingenieur, **11** (1940). 6–20

[6] K. Pietrak, T. S. Wisniewski: J. Power Technol. **95** (2014) 14-24.

[7] D. P. H. Hasselman, L. F. Johnson: J. Compos. Mater. **21** (1989) 508-515.

[8] J.D. Eshelby: Roy. Soc. London A **241** (1957) 376.

[9] R. Tavanger, J. M. Molina, L. Weber: Scr. Mater. **56** (2007) 357-360.

[10] T. Mori, K. Tanaka: Acta Met. **21** (1973) 571-574.

[11] J. Stransky, J. Vorel, J. Zeman, M. Sejnoha: Micromachines. **8** (2011) 1-21.

[12] C.W. Nan, Z. Shi and Y. Lin: Chem. Phys. Lett. **375** (2003) 666–669.

[13] C.W. Nan, G. Liu, Y. H. Lin and M. Li: Appl. Phys. Lett. **85** (2004) 3549-3551.

[14] ANSYS, Inc., USA, Available at. https://courses.ansys.com/wp-content/uploads /2020/12/LT4C1-Lesson4-Handout-NT_v2.pdf (Accssed 2022-11-26).

[15] Y. A. Cengel, A. J. Ghajar: Heat and Mass Transfer: Fundamentals & Applications (McGraw Hill, Inc. USA, 2011) pp. 75-77

Chapter 5

Conclusions

With the rapid development of electronic device, traditional TIMs cannot meet the requirements of advanced electronic devices due to their low thermal conductivity and other poor properties. In the previous studies, although advanced carbon TIMs were developed successfully with better physical properties and characteristics like higher thermal conductivity, light-weight property, better physical and mechanical stability compared to traditional TIMs, the properties of these carbon TIMs still cannot not be completely exploited and required complex manufacturing process and high cost, which was too difficult to be applied in practical applications due. The object of this thesis is to fabricate CNF sheets by using conductive fillers VGCF and PVA binder that exhibit high thermal conductivity by simple and low-cost fabrication process. Furthermore, as an attempt to increase the functionality for practical application, PTFE particles were added to fabricated PVA-PTFE-VGCF sheets for an improvement in hydrophilicity. The thermal simulations were measured to evaluate the heat transfer paths in CNF sheet and develop a method for predicting thermal conductivity by using data of thermal simulation. The conclusions of this thesis are summarized as follows:

(1) An innovative TIM consisting of PVA and VGCF was fabricated successfully, by a simple and simply and cost-efficient solution casting method (Chapter 2). 5 kind of CNF sheets were fabricated with different mass ratio of PVA:VGCF: 1:0.1(17.04 vol.%), 1:0.07(12.85 vol.%), 1: 0.05 (10.15 vol.%), 1: 0.03 (8.18 vol.%), 1: 0.025 (7.95 vol. %). Microstructure observation revealed that the VGCFs were arranged in random directions and interconnected via PVA aggregates. Numerous pores existed between the VGCFs due to water evaporation. The porosity of the CNF sheets decreased by decreasing the VGCF amount. The thickness of the CNF sheets was between 30 - 56 μm and increased with increasing the VGCF amount. Moreover, the CNF sheets did not

exhibit considerably different density and hardness: the average density of the CNF sheet was about 1.00×10^6 g·m^3, the Shore hardness of the CNF sheets was between 82 - 85 HS. It is indicated CNF sheets was fabricated with suitable thickness, lightweight property and great flexibility for practical application of TIM.

The highest value of thermal conductivity was obtained for the CNF sheet fabricated at the PVA:VGCF mass ratio of 1:0.050, with the in-plane and through-plane thermal conductivities being 14.30 and 6.44 $W \cdot m^{-1} \cdot K^{-1}$, respectively. Reducing the VGCF amount decreased the thermal conductivity. Furthermore, an excessive increase in the VGCF amount increased the number of pores in the CNF sheet, which led to thermal conductivity reduction. The in-plane and through-plane thermal conductivities were significantly reduced after the high-temperature and humidity tests. It is considered that due to the hydrophilic property of PVA, the water molecules in the environment would be absorbed into CNF sheet by PVA, which led to high porosity and thermal conductivity reduction.

(2) For an improvement in hydrophilicity, PPVL and PPTV sheets were fabricated by using 120nm and 300nm PTFE particle (Chapter 3). The microstructure observation of PPLV and PPTV revealed that the VGCFs were arranged in random directions and interconnected via PVA aggregates, which similar to PVA-VGCF sheet. 300nm PTFE particles were well distributed and compatible within the PPTV sheet, while partial aggregations of 120nm PTFE particles and unfilled pores were observed in the PPLV sheet. As the pores on the surface were filled by PTFE powders, the porosity of the fabricated sheet was reduced. The average thickness of the fabricated sheets was also decreased from 47μm for the PVA-VGCF sheet to 31.2μm and 28.2μm for PPLV and PPTV sheets respectively, due to the lower content of the PVA matrix.

With the addition of 300nm PTFE particles, the fabricated sheet has higher thermal conductivities of 9.81 $W \cdot m^{-1} \cdot k^{-1}$ in the in-plane direction and 2.11 $W \cdot m^{-1} \cdot k^{-1}$ in the through-plane direction. The in-plane and through-plane TC of PVA-PTFE-VGCF sheets were decreased by 31% ~ 46% and 67% ~ 72% compared with referred PVA-VGCF sheet, due to the thermal barrier of PTFE particles. In the high temperature and humidity test under the condition of 358K and 85% RH, the in-plane and through-plane

TC of PVA-PTFE-VGCF sheets were increased by 10% ~ 18% and 18% ~ 23%. According to the FT-IR analysis result, it is considered that the increase in TC was caused by the hydrophobic property of PVA and rearrangement of PVA and PTFE particles.

(3) 5 types of materials models were created successfully: pure PVA, horizontally arranged VGCF in PVA matrix, vertically arranged VGCF in PVA matrix, randomly arranged VGCF in PVA matrix and pure VGCF (Chapter 4). To investigate the heat transfer path and thermal conductivity of them, these material models were combined with a heater and a cooler to measure the thermal simulations. Material models of pure PVA, horizontally arranged and vertically arranged VGCF in PVA showed a similar distribution of temperature. The change of temperature was mainly concentrated on the region of the test material which dropped from 363K to 303K. Temperature distribution of randomly arranged VGCF model had obvious fluctuations along the VGCF direction. To material model of pure VGCF, the temperature distribution exhibited a uniform distribution from top of heater to bottom of cooler.

Pure PVA and pure VGCF models had the constant heat flux distribution value respectively due to their single-phase microstructure. Due to lacking efficient heat transfer path, the material model of horizontally arranged VGCF showed very low heat flux data, which was almost similar to pure PVA. As for the model of vertically arranged VGCF, each single vertical VGCF connected heater and cooler, which provided many efficient heat transfer paths for the materials. The efficient heat transfer paths in material model of randomly arranged VGCF were created only by the interleaved VGCFs and connections of each other.

In the calculation of thermal conductivity by using thermal simulation results, the material models of pure PVA and pure VGCF exhibited the lowest thermal conductivity(PVA: 0.497 $W \cdot m^{-1} \cdot K^{-1}$) and the highest thermal conductivity(VGCF: 1193.749 $W \cdot m^{-1} \cdot K^{-1}$), respectively. The material model of horizontally arranged VGCF exhibited the almost the same low thermal conductivity(0.509 $W \cdot m^{-1} \cdot K^{-1}$) as pure PVA. The material model of vertically arranged VGCF, its thermal conductivity was as high as 8.238 W·m-1·K-1 due to efficient heat transfer paths. As for the material model of

randomly arranged VGCF, which had a similar microstructure with fabricated PVA-VGCF sheet, the thermal conductivity of 4.600 $W \cdot m^{-1} \cdot K^{-1}$, and the thermal conductivity of this model can be improved significantly by increasing the amount of VGCF.

Acknowledgements

I would like to dedicate my paper to all those who have offered me tremendous assistance.

First of all, my heartiest thanks flow to my supervisor, Associate Professor Choi, for his helpful guidance, valuable suggestions, and constant encouragement both in my study and in my life. His profound insight and accurateness about my paper taught me so much that they are engraved on my heart. He provided me with beneficial help and offered me precious comments during the whole process of my writing, without which the paper would not be what it is now.

Also, I would like to express my sincere gratitude to Professor Matsugi, who have taught me in this university that greatly broadened my horizon and enriched my knowledge in my study. His inspirational and conscientious teaching have provided me with a firm basis for the composing of this paper and will always be of great value to my future academic research. In addition, I would like to express my heartfelt thanks to Professor Inumaro and Professor Akebono for their technical advice and assistance to my doctoral thesis.

My thanks also go to the members of my lab whose monographs and academic ideas have enlightened me in my whole research life.

Finally, I would like to extend my deep gratefulness to my family and friends, especially my fiancée Siran Chen, who encouragement and support have made my accomplishments possible.

Published papers in regard to this thesis

1. **J. L. Xiong**, S. R. Chen, Y. B. Choi*, K. Matsugi. Development of polyvinyl alcohol-based carbon nano fiber sheet for thermal interface material. Scientific reports. 2021(11) 17183. (Chapter 2)

2. **J. L. Xiong**, T. Kinoshita, Y. B. Choi*, K. Matsugi, Y. Hisazato, N. Fujiwara. Thermal Properties of Carbon Nanofiber Sheet for Thermal Interface Materials under High Temperature and Humidity. Materials transactions. 2023 (64): in press. (Chapter 3)

Presentations

1. **Jiangling Xiong**, Siran Chen, Yongbum Choi, Kazuhiro Matsugi. Fabrication of carbon nano fiber sheet for thermal interface material. 2021 2nd Japan-Korea collaborative Symposium in Advanced Composite Materials. Sep. 10, 2021, Hiroshima, Japan; Hiroshima University.

2. **Jiangling Xiong**, Siran Chen, Tomoo Kinoshita, Yongbum Choi, Kazuhiro Matsugi, Yuuji Hisazato, Nobuto Fujiwara. Performance evaluation of carbon nanofiber interface material. May 22-26, 2022, Matsue, Janpan.